ADVANCED MISSION DESIGN: INTERPLANETARY SUPER HIGHWAY TRAJECTORY METHOD

A Dissertation

by

HYERIM KIM

Submitted to the Office of Graduate and Professional Studies of
Texas A&M University
in partial fulfillment of the requirements for the degree of

DOCTOR OF PHILOSOPHY

Chair of Committee,	David C. Hyland
Committee Members,	Srinivas Rao Vadali
	Tom Pollock
	Lucas Macri
Head of Department,	Rodney Bowersox

August 2015

Major Subject: Aerospace Engineering

ABSTRACT

Near-future space missions demand the delivery of massive payloads to deep space destinations. Given foreseeable propulsion technology, this is feasible only if we can design trajectories that require the smallest possible propulsive energy input. This research aims to design interplanetary space missions by using new low-energy trajectory methods that take advantage of natural dynamics in the solar system. This energy efficient trajectory technology, called the Interplanetary Super Highway (IPSH), allows long duration space missions with minimum fuel requirements. To develop the IPSH trajectory design method, invariant manifolds of the three-body problem are used. The invariant manifolds, which are tube-like structures that issue from the periodic orbits around the L_1 and L_2 Lagrangian points, can be patched together to achieve voyages of immense distances while the spacecraft expends little or no energy. This patched three-body method of trajectory design is fairly well developed for impulsive propulsion. My research is dedicated to advance its capabilities by extending it to continuous, low-thrust, high specific impulse propulsion methods.

The IPSH trajectory design method would be useful in designing many types of interplanetary missions. As one of its applications, my research is focused on Near-Earth Asteroids (NEAs) rendezvous mission design for exploration, mitigation, and mining. Asteroids have many valuable resources such as minerals and volatiles, which can be brought back to Earth or used in space for propulsion systems or space habitats and stations. Transportation to and from asteroids will require relatively massive vehicles

capable of sustaining crew for long durations while economizing on propellant mass. Thus, in the design of advanced NEA rendezvous missions, developing new technology for low cost trajectories will play a key role.

In a second application study, the solar sail mission for Mars exploration is considered. By using solar radiation pressure, solar sails provide propulsive power. This thrust affects the three-body system dynamics such that the Sun-Mars L_1 and L_2 Lagrangian points are shifted toward the Sun and the geometry of the invariant manifolds around L_1 and L_2 points is changed. By taking advantage of these features, a low-thrust trajectory for Mars exploration is developed.

ACKNOWLEDGEMENTS

I would like to thank Dr. David C. Hyland for his contributions and exceptional mentorship through the course of this research. He has motivated and encouraged me with valuable discussions on this topic.

Also I would like to thank to my colleagues who have consistently helped my graduate study at Texas A&M University: Shen Ge, Micaela Landivar, Richard Margulieux, Julie Sandberg, Neha Satak, Russell Trahan, and Brian Young.

Finally, thanks to my mother and father for their infinite support and to my wonderful husband for his unconditional trust and love.

NOMENCLATURE

BCM	Bi-Circular Model
C	Jacobi Integral
CCM	Concentric Circular Model
DCM	Differential Correction Method
E	Energy Integral
f	Solar Sail Factor
GEO	Geosynchronous Equatorial Orbit
I_{sp}	Specific Impulse
IPSH	Interplanetary Super Highway
LEO	Low Earth Orbit
NEA	Near-Earth Asteroid
PCR3BP	Planar Circular Restricted 3-Body Problem
r_h	Hill Radius
S/C	Spacecraft
STM	State Transition Matrix
U	Pseudo-Potential Energy Function
$\bar{U}$	Effective Potential Energy Function
μ	Mass Parameter

TABLE OF CONTENTS

Page

LIST OF FIGURES

Page

LIST OF TABLES

Page

1. INTRODUCTION

Over the last half-century, many successful space missions have been launched. Most interplanetary mission trajectories have been designed through the traditional conic solution with the dynamical principles of the 2-body problem. For example, a Hohmann transfer, which is one of the simple solutions for the 2-body problem, has been used in many successful missions. However, it is not always practical and has limits in hardware capabilities and cost. By increasing the demand for new design technology which meets complex mission scenarios and economical requirements of using minimum fuel, many investigations have focused on low-energy trajectory methods. The Interplanetary Super Highway (IPSH) trajectory method, one of the well-known low-thrust trajectory methods, was developed based on the Circular Restricted 3-BodyProblem (CR3BP) [1]. The CR3BP can take advantage of natural dynamics using invariant manifolds which can connect around Lagrangian points like a chain of tunnels [1-4]. This dissertation explores the dynamics of CR3BP and is focused on designing energy efficient trajectories for interplanetary missions.

1.1 Historical Contributions

One of the remarkable contributions to the 3-body problem was started by two mathematicians, Leonhard Euler (1767) and Joseph-Louis Lagrange (1772) with identification of five equilibrium points in the restricted 3-body problem. Euler proposed the restricted 3-body problem in a rotating frame [5]. This model became the basic

foundation of recent researches on CR3BP. He discovered three collinear points (L_1, L_2, L_3) first and then Lagrange defined two equilateral points (L_4, L_5) later. Those five equilibrium points are commonly known as "Lagrangian points" or "libration points". An object in the vicinity of Lagrangian points will be in a state of equilibrium [6]. These points have a significant role in the transfer trajectory design since the existence of periodic orbits and the tunnels around the points are discovered in later work.

Another significant contribution was made by Carl Gustave Jacob Jacobi (1836) who discovered the Jacobi constant. His works focused on the integral of motion in the 3-body problem [7]. By extending Jacobi's work, George William Hill (1878) modeled the lunar orbit considering the effect of Sun. He demonstrated that the existence of regions which limit the motion of third body depends on the energy level [8]. These region called Hill's curves of zero velocity defined the realms of the forbidden zone where the third body cannot enter.

One of the innovative approaches to CR3BP was developed by Henri Poincare in the 19^{th} century. He studied a natural motion of PCR3BP in its qualitative aspects with a surface section method called the Poincare section [9]. Based on these advances and the advent of modern computers, several space missions have been designed and launched based on 3-body problem. The first one was the ISEE-3 mission which transferred a spacecraft to a periodic orbit around Sun-Earth L_1 point in 1978 [10, 11]. After that numerical techniques were combined with CR3BP by many researchers in the 1990s. Especially, the design algorithms developed by Wilson, Barden, and Howell were implemented in the Genesis Discovery mission which was launched in 2001 [12].

Collecting a sample of solar wind particles, the spacecraft reached the Sun-Earth L_1 orbit and came back to Earth with significantly low thrust. The Genesis mission manifested the usefulness of low energy transfer trajectories associated with invariant manifolds around Lagrangian points.

1.2 Problem Statement

Various techniques for low thrust trajectory design were proposed and developed over the last few decades. Among them, interplanetary transfer trajectory design methods associated with the invariant manifolds around Lagrangian points are one of the noted energy efficient trajectory design methods. In the restricted 3-body system formulation it is assumed that two massive particles move in their circular orbits while a third body of negligible mass freely moves around them in the same orbit plane without affecting the motion of two massive bodies. This simplified situation, called the Planar Circular Restricted 3-Body Problem (PCR3BP), leads us to fruitful insights into the motion of three bodies. By understanding of dynamics and energy states of 3-body system, a reasonably tractable mathematical model can be defined for the PCR3BP. However it is still challenging to obtain the solutions of transfer trajectory designs. A large amount of computationally precise effort is needed due to the high sensitivity of trajectories to initial conditions. To deal with this complex control problem, many different types of efficient tools were studied by Belbruno [13, 14], Howell [15], and Lo [1-4]. To find a systematically general and simple solution of PCR3BP, this research has focused on developing a new design approach, called 1-D search techniques in PCR3BP.

Furthermore, the results of this work may offer insight for the global structure of invariant manifolds and possibilities of advanced trajectory design.

The basic background of the PCR3BP is introduced in Section 2 to provide the foundations of this study. The mathematical model of PCR3BP is developed based on the work of Conley [16] and W. S. Koon [1]. The energy states of the PCR3BP including the Jacobi integral and Hill's region are also discussed.

In Section 3, the invariant manifolds are investigated to understand the geometry of the multi-body problem. We developed the 1-D search method associated with the dynamics of PCR3BP. To compare with the 1-D search method, the general numerical method, specifically the differential correction method (DCM), is also reviewed. The results of preliminary trajectory design for NEA rendezvous mission are presented.

In Section 4, we explore the special case of the 4-body problem which can be useful for Mars exploration. Assuming the use of solar sails, we studied the resulting changes in the natural motion and geometric structure in the restricted 4-body problem. A sample transfer trajectory from Earth to Mars is presented.

In Section 5, we make concluding remarks and discuss recommendations for further investigations.

2. BACKGROUND: MATHEMATICAL MODEL

2.1 The N-Body Problem

Suppose that there are three bodies m_1, m_2, and m_3 all executing circular motions in the same plane. Then typical motions can be described in two ways. First, when m_2 and m_3 move in circular orbits around m_1 as a center, as shown on the left in Figure 1, we call this Concentric Circular Model (CCM) [1]. This model can be applied to any interplanetary system within the solar system, such as the Sun-Earth-Mars system. Second, consider m_2 and m_3 to be in relatively small circular motions about their barycenter and that the m_2-m_3 barycenter is in a large circular orbit about m_1. This situation, shown on the right in Figure 1, is called the Bi-Circular Model (BCM) [1]. This model can be applied to planet-satellite system with the Sun such as Sun-Earth-Moon system. For Near Earth Asteroid (NEA) mission design, the BCM will be considered to produce an Earth to Asteroid trajectory via the Earth-Moon system to the Sun-Earth system. The CCM will be considered to describe the Sun-Earth-Mars system.

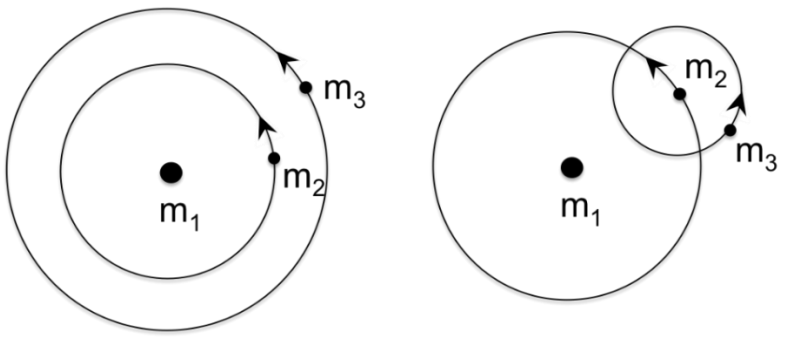

Figure 1. Concentric circular model (left) and bi-circular model (right)

To describe the motion of the third body, m_3 effectively, let us explore the reference frames in the three-body system. In Figure 2, assume that the inertial frame is the X-Y plane which is the orbital plane of the two primaries. Since those two bodies are constantly moving, it is inconvenient to formulate the equation of motion for m_3 in the inertial frame. Let us consider the m_1-m_2 rotating reference frame which is consist of the x-y plane in Figure 2. Note that the x-y frame rotates with the angular velocity of the primaries with respect to the X-Y frame. The transformation from inertial to rotating frame can be helpful to represent the equation of motion in PCR3BP.

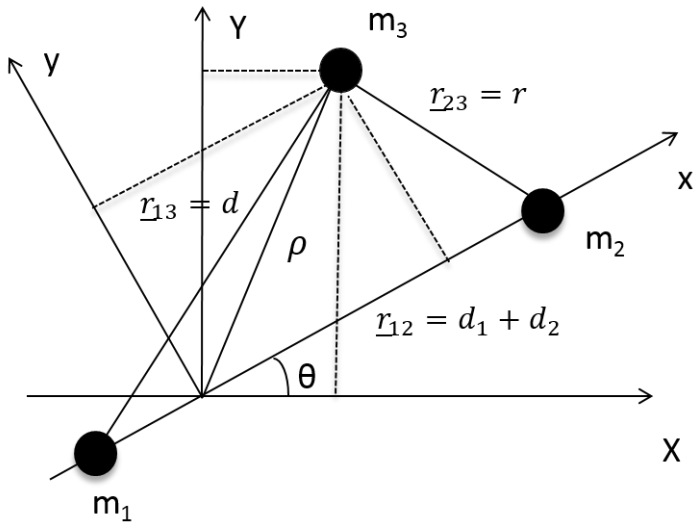

Figure 2. The n-body problem in inertial frame and rotating frame

2.2 Normalized Units

For the three-body problem in this research, the system units were used as non-dimensional quantities. By generalizing the equation of motion with the normalized unit,

it is more convenient to describe the motion of bodies composing different systems. The fundamental parameters to be normalized in the system are length L, mass M, and time t. The unit of length, L is defined as the distance between the two primary bodies, m_1 and m_2, i.e. $L = d_1 + d_2$ in Figure 2. The unit of mass, M is defined as the summation of mass, $M = m_1 + m_2$. The unit of time, t can be calculated assuming the orbital period of m_1 and m_2, called T, is 2π. So the conversion of those fundamental quantities into the normalized unit can be described as:

$$d' = Ld \tag{2.1a}$$

$$t' = \frac{T}{2\pi} t \tag{2.1b}$$

where d', t' are the dimensional units and d, t are the non-dimensional units for length and time respectively. Especially the mass parameter, μ can be represented as:

$$\mu = \frac{m_2}{m_1 + m_2} \tag{2.2}$$

In the case that m_1 is larger than m_2, the non-dimensional mass of the first and second primaries are expressed as:

$$\mu_1 = 1 - \mu, \qquad \mu_2 = \mu \tag{2.3}$$

Note that the mass parameter μ and dimensional values of length L, velocity V, and the orbital period T in various interplanetary systems are shown in Table 1. Those values are provided from the Jet Propulsion Laboratory's solar system dynamics website [1].

Table 1. The dimensional units of fundamental quantities in the solar system [1]

System	μ	L	V	T
Sun-Jupiter	9.537×10^{-4}	7.784×10^{8}	13.102	3.733×10^{8}
Sun-(Earth+Moon)	3.036×10^{-6}	1.496×10^{8}	29.784	3.147×10^{7}
Earth-Moon	1.215×10^{-2}	3.850×10^{5}	1.025	2.361×10^{6}
Mars-Phobos	1.667×10^{-8}	9.380×10^{3}	2.144	2.749×10^{4}
Jupiter-Io	4.704×10^{-5}	4.218×10^{5}	17.390	1.524×10^{5}
Jupiter-Europa	2.528×10^{-5}	6.711×10^{5}	13.780	3.060×10^{5}
Jupiter-Ganymede	7.804×10^{-5}	1.070×10^{6}	10.909	6.165×10^{5}
Jupiter-Callisto	5.667×10^{-5}	1.883×10^{6}	8.226	1.438×10^{6}
Saturn-Mimas	6.723×10^{-8}	1.856×10^{5}	14.367	8.117×10^{4}
Saturn-Titan	2.366×10^{-4}	1.222×10^{6}	5.588	1.374×10^{6}
Neptune-Triton	2.089×10^{-4}	3.548×10^{5}	4.402	5.064×10^{5}
Pluto-Charon	1.097×10^{-1}	1.941×10^{4}	0.222	5.503×10^{5}

2.3 Equation of Motion for PCR3BP

In PCR3BP, we assume that a spacecraft m_3 freely moves around the gravitational field governed by two massive bodies m_1 and m_2. All three bodies move in the same plane and the two primaries are in circular orbit about their center of mass. The position, velocity and acceleration for the m_3 can be written in the m_1-m_2 rotating reference frame [6].

$$\underline{+R\rho} = x\,\hat{x} + y\hat{y} + z\hat{z} \tag{2.4a}$$

$$+i\underline{\dot{\rho}} = +R\underline{\dot{\rho}}x + \left(\underline{\omega}_{R/i} \times \underline{\rho}\right) = \left(\dot{x} - \dot{\theta}y\right)\hat{x} + \left(\dot{y} + \dot{\theta}x\right)\hat{y} + \dot{z}\hat{z} \tag{2.4b}$$

$$+i\underline{\ddot{\rho}} = +R\underline{\dot{\rho}} + (\,\underline{\omega}_{R/i} \times +R\underline{\dot{\rho}}) = (\ddot{x} - 2\dot{y} - x)\hat{x} + (\ddot{y} + 2\dot{x} - y)\hat{y} + \ddot{z}\hat{z} \tag{2.4c}$$

where the position ρ, velocity$\underline{\dot{\rho}}$, and acceleration $\underline{\ddot{\rho}}$ in the rotating frame, $+R$, and inertial frame, $+i$, respectively. Also we assume that the non-dimensional angular velocity $\underline{\omega}_{R/i} = \dot{\theta} = 1$ which means the frame rotates at a fixed rate.

Let us consider a Newtonian approach to describe the force equation for m_3. The law of motion with total force acting in the three-body problem can be represented as:

$$\underline{F}_i = m_i \underline{\ddot{r}}_i = \sum_{j=1}^{n} \frac{G m_i m_j}{{r_{ij}}^3} \underline{r}_{ij} \quad (i \neq j,\ n = 3) \tag{2.5}$$

where G is a universal gravitational constant, $6.67384e^{-11}$ $m^3kg^{-1}s^{-2}$, F is the force acting on each body, and $\underline{\ddot{r}}_i$ is the acceleration vector in the inertial frame [17]. The equation of third body motion can be written as:

$$\underline{F}_3 = m_3 \underline{\ddot{r}}_i = \frac{G m_3 m_1}{{r_{31}}^3} \underline{r}_{31} + \frac{G m_3 m_2}{{r_{32}}^3} \underline{r}_{32} \tag{2.6}$$

In Figure 2, we can find the geometric relationships such that $\underline{r}_{31} = -\underline{d}$, $\underline{r}_{32} = -\underline{r}$. By using the non-dimensional units of length and time that we defined in section 2.2, the position vectors can be normalized.

$$\mathrm{L} = d_1 + d_2 = \underline{r}_{12} \tag{2.7a}$$

$$t^* = \sqrt{\frac{L^3}{G(m_1 + m_2)}} \tag{2.7b}$$

$$\begin{cases} \underline{d} = \frac{\underline{r}_{13}}{L} \\ \underline{r} = \frac{\underline{r}_{23}}{L} \\ \underline{\rho} = \frac{\underline{r}_3}{L} \end{cases} \tag{2.7c}$$

By multiplying $(t^*)^2$/L and eliminating m_3 in the equation (2.6), it can be expressed as:

$$\frac{d^2\left(\underline{r}_3/L\right)}{d\left(t/t^*\right)^2} = \frac{Gm_1}{{r_{31}}^3}\left(\frac{(t^*)^2}{L}\right)\underline{r}_{31} + \frac{Gm_2}{{r_{32}}^3}\underline{r}_{32}\left(\frac{(t^*)^2}{L}\right) \tag{2.8}$$

To the above equation, we can apply the equation (2.7c). Then, the Newton's law of motion can be described as:

$$\frac{d^2\rho}{d\tau^2} = \frac{Gm_1(t^*)^2}{{r_{31}}^3}\underline{d} + \frac{Gm_2(t^*)^2}{{r_{32}}^3}\underline{r} \tag{2.9}$$

where the position vector $\underline{r}_3 = \rho$ and the non-dimensional time is defined as $\tau = t/t^*$. Then t^* can be substituted using the equation (2.7b). The acceleration vector, $\underline{\ddot{\rho}}$ in the inertial frame can be rewritten as:

$$\frac{d^2\rho}{d\tau^2} = -\frac{(1-\mu)}{d^3}\underline{d} - \frac{\mu}{r^3}\underline{r} \tag{2.10a}$$

$$\underline{d} = (x+\mu)\hat{x} + y\hat{y} + z\hat{z} \tag{2.10b}$$

$$\underline{r} = (x-1+\mu)\hat{x} + y\hat{y} + z\hat{z} \tag{2.10c}$$

The normalized position vectors, $\underline{d}$ and $\underline{r}$ can be expressed in the x-y coordinate of the rotating frame. By combining the results of the equation (2.4c) and (2.10a), the following scalar, second-order, nonlinear set of differential equations is obtained.

$$\hat{x}: \quad (\ddot{x} - 2\dot{y} - x) = -\frac{(1-\mu)}{d^3}(x+\mu) - \frac{\mu}{r^3}(x-1+\mu) \tag{2.11a}$$

$$\hat{y}: \quad (\ddot{y} + 2\dot{x} - y) = -\frac{(1-\mu)}{d^3}y - \frac{\mu}{r^3}y \tag{2.11b}$$

$$\hat{z}: \quad \ddot{z} = -\frac{(1-\mu)}{d^3}z - \frac{\mu}{r^3}z \tag{2.11c}$$

Let us define the pseudo-potential energy function, U as:

$$U = \frac{1}{2}(\dot{x}^2 + \dot{y}^2) + \frac{1-\mu}{d} + \frac{\mu}{r} \tag{2.12}$$

Then we can derive the equations of motion for m_3 relative to the m_1-m_2 rotating reference frame in non-dimensional coordinates.

$$\ddot{x} - 2\dot{y} = \frac{\partial U}{\partial x} \tag{2.13a}$$

$$\ddot{y} + 2\dot{x} = \frac{\partial U}{\partial y} \tag{2.13b}$$

$$\ddot{z} = \frac{\partial U}{\partial z} \tag{2.13c}$$

Also the above equation can be expressed in the first-order form. By considering the planar circular motion on x-y plane, we can obtain the simplified equation of motion for the PCR3BP.

$$\dot{x} = v_x \tag{2.14a}$$

$$\dot{y} = v_y \tag{2.14b}$$

$$\dot{v_x} = 2v_y - \frac{\partial \bar{U}}{\partial x} + F_x \tag{2.14c}$$

$$\dot{v_y} = -2v_x - \frac{\partial \bar{U}}{\partial y} + F_y \tag{2.14d}$$

where the effective potential $\bar{U} = -\frac{1}{2}(x^2 + y^2) - \frac{1-\mu}{r_1} - \frac{\mu}{r_2}$; $r_1 = \sqrt{(x+\mu)^2 + y^2}$, $r_2 = \sqrt{(x-1+\mu)^2 + y^2}$; F_x, F_y = x, y components of thrust.

2.4 Equilibrium Points in PCR3BP

To find equilibrium points in the PCR3BP, we assume that both velocity and acceleration relative to the rotating frame are zero. Let us set the right-hand sides of equation (2.14) to zero, i.e. $\dot{x} = \dot{y} = \dot{v_x} = \dot{v_y} = 0$ and Fx = Fy = 0. Then the position of the equilibrium points in the PCR3BP can be determined: 1) three unstable points on the

x-axis, called L_1, L_2, and L_3, form a collinear formation solution 2) two stable points, called L_4 and L_5, form an equilateral triangle solution. These five equilibrium points, commonly referred as the Lagrange points, are illustrated in Figure 3.

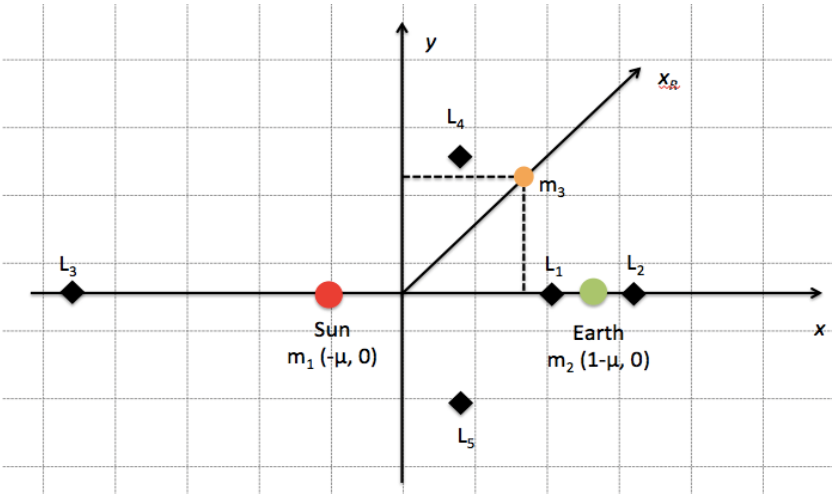

Figure 3. Lagrange points L_i, i=1,…,5 in PCR3BP

If the third body, m_3, is placed at the equilibrium points with zero velocity, it will remain at rest in the rotating frame. Therefore these points are useful for various space missions as a connecting hub or observing destination. Especially, the existence of the periodic orbit around the L_1 and L_2 points is an important feature to IPSH trajectory design method. More details will be discussed in following section in this paper.

To calculate the collinear equilibrium points, the critical condition for the effective potential function $\bar{U}$ is:

$$\frac{d}{dx}\left(\bar{U}(x,0)\right) = -x + \frac{1-\mu}{(x-\mu)^2} + \frac{\mu}{(x-1+\mu)^2} = 0 \qquad (2.15)$$

Let the position x be $\delta + 1 - \mu$ where the separated distance from the second primary, δ is negative for the L_1 point and positive for the L_2 point. By substituting $\delta + 1 - \mu$ for x making δ the unknown, the equation (2.15) can be represented as:

$$L_1: \qquad \delta = -\left(\frac{\mu(1+\delta)^2+(1-\mu)\delta^4}{(1+\delta)^2+2(1-\mu)}\right)^{\frac{1}{3}} \cong -r_h = -(\frac{\mu}{3})^{1/3} \tag{2.16a}$$

$$L_2: \qquad \delta = \left(\frac{\mu(1+\delta)^2-(1-\mu)\delta^4}{(1+\delta)^2+2(1-\mu)}\right)^{\frac{1}{3}} \cong r_h = (\frac{\mu}{3})^{1/3} \tag{2.16b}$$

Where r_h, denotes the Hill radius, which is the radius of the Hill's region in the PCR3BP. Equations (2.16) represent iterative sequences wherein, starting at zero, successive values of δ are substituted into the right-hand sides to generate the next iterates. These sequences are rapidly convergent.

2.5 Energy State Dynamics: Jacobi Constant, Hill's Region

The motion of the particle, m_3, is impossible when its kinetic energy is negative. This impenetrable area, called the forbidden zone, can be calculated by the energy integral of motion, E (C=-2E, C is Jacobi integral). This energy integral can exist since the equation of motion for the PCR3BP are Hamiltonian and time independent. The energy integral can be expressed as a function of the position and velocities.

$$E = \frac{1}{2}\left(\dot{x}^2 + \dot{y}^2\right) + \bar{U} \tag{2.17}$$

Based on this energy level, we can divide the phase space of the PCR3BP into five possible cases. As seen in Figure 4, a projection of the energy surface, called the Hill's region, can be plotted in the blue zone, while the forbidden realm is shown in red zone. The five cases are divided based on a critical energy levels E_i i=1,..,5 which

correspond to the energy of a particle at rest at the Lagrange point L_i, i=1,…,5. For example, the spacecraft m_3 cannot move between the m_1 and m_2 regions due to lower energy than E_1. By increasing the energy level, the neck region between m_1 and m_2 regions will be opened up. If the energy of spacecraft is slightly above E_2 such as case 3, m_3 can move around the realm of m_1 and m_2, even the exterior realm too.

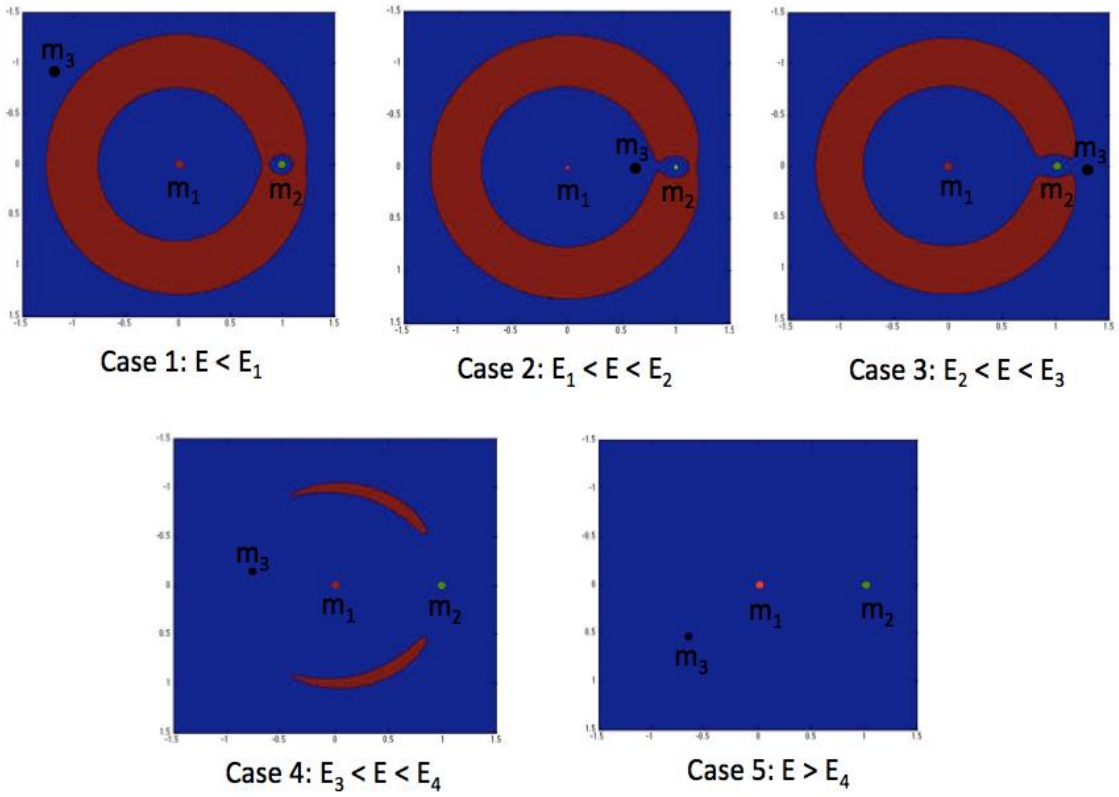

Figure 4. Five possible motions for energy state phase of the PCR3BP

3. DESIGN TRAJECTORY WITH GEOMETRY OF N-BODY PROBLEM

3.1 Invariant Manifolds

The investigation of invariant manifolds was developed by the French mathematician Henri Poincare who was dedicated to the study of abstract dynamical stability of systems in the late 19^{th} century [9]. Based on his mathematical foundation, later researchers focused on mapping the geometry of the N-body system. A geometrical view for the N-body system considers the set of all possible states of the system in the phase space. Among the possible sets of trajectories, one can discern trajectory sets that trace out all the points in a connected subspace of phase space. Such a set is called an invariant manifold, which is a cylinder type tube structure winding around the equilibrium points in the N-body system. Particles can be transported through the invariant manifolds between large regions of the energy surface by winding around the periodic orbits near L_1 and L_2, called Lyapunov orbits. The characteristics of the invariant manifolds issuing from the periodic orbits is investigated in this section.

To generate invariant manifolds, it is necessary to do numerical computation. First the traditional computation method is examined briefly, then an advanced but simple method is addressed in detail. Commonly the Differential Correction Method (DCM) used to generate the Lyapunov orbit and associated manifolds are accurate enough for space mission design. This method consists in successive approximations using the State Transition Matrix (STM) along with a reference trajectory [19, 20]. For the first period of a Lyapunov orbit, the STM is called the monodromy matrix, Φ. The

eigenvalues and eigenvectors of the monodromy matrix determine the characteristics of the local geometry in the system. Given the eigenvectors of the monodromy matrix, the initial guess of the stable manifold, X_s and unstable manifold, X_u can be described as:

$$X_s = x_0 + dV_s \tag{3.1a}$$

$$X_u = x_0 + dV_u \tag{3.1b}$$

where V_s and V_u denote the stable and unstable eigenvectors, respectively, of the monodromy matrix at point x_0, and d is initial displacement. By integrating the equation of motion for PCR3BP with the different initial positions along the periodic orbit, the local approximation of the stable and unstable manifolds can be calculated. As an example, let us consider the Lyapunov orbit around the Earth-Moon L_1 point [21]. In Figure 5, both unstable (red) and stable (blue) manifolds are illustrated. Both manifolds which are departing (unstable) and approaching (stable) to the periodic orbits are generated by the position components for 50 different points along the orbits.

The Eigen-basis of the system dynamics can provide simple portraits of the Lyapunov orbits. By following the centerline of the invariant manifolds, the global form of these tubes can be simply mapped. Let us assume that the radius of the Lyapunov orbit approaches zero. Then the resulting one-dimensional paths imply the proper initial conditions to the interior and exterior realm. These trajectories are the minimum energy paths within the tubes. By taking a small perturbation in the direction of the eigenvector, the initial one-dimensional trajectory initially following the periodic orbit enclosing the Lagrange point evolves to form tube-like surface, as illustrated in Figure 6. Two sets of

initial conditions respectively with the interior and exterior directions for the stable and unstable manifolds are shown in Table 2. Note that α is very small positive constant.

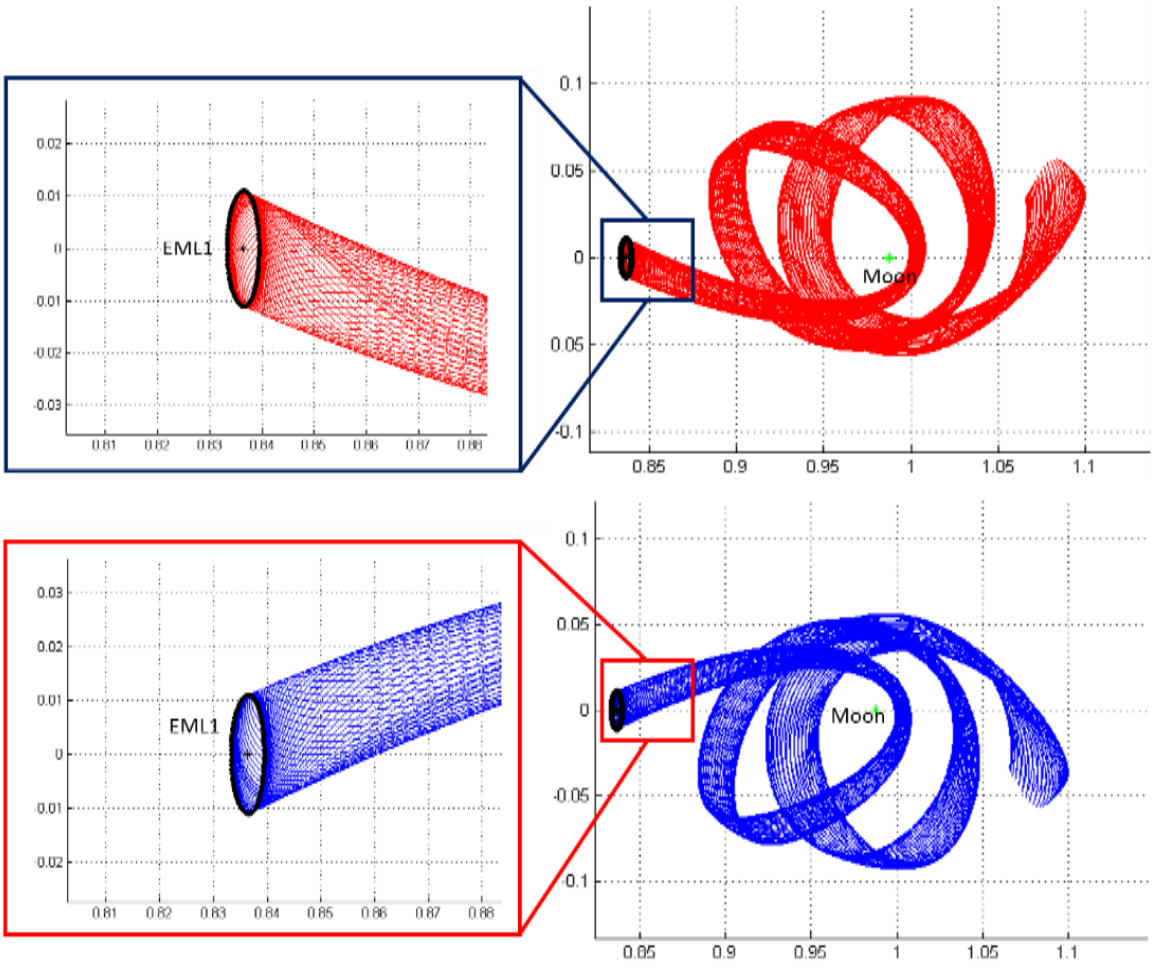

Figure 5. Unstable (red, top) and stable (blue, bottom) manifolds from the periodic orbits around Earth-Moon L_1 point

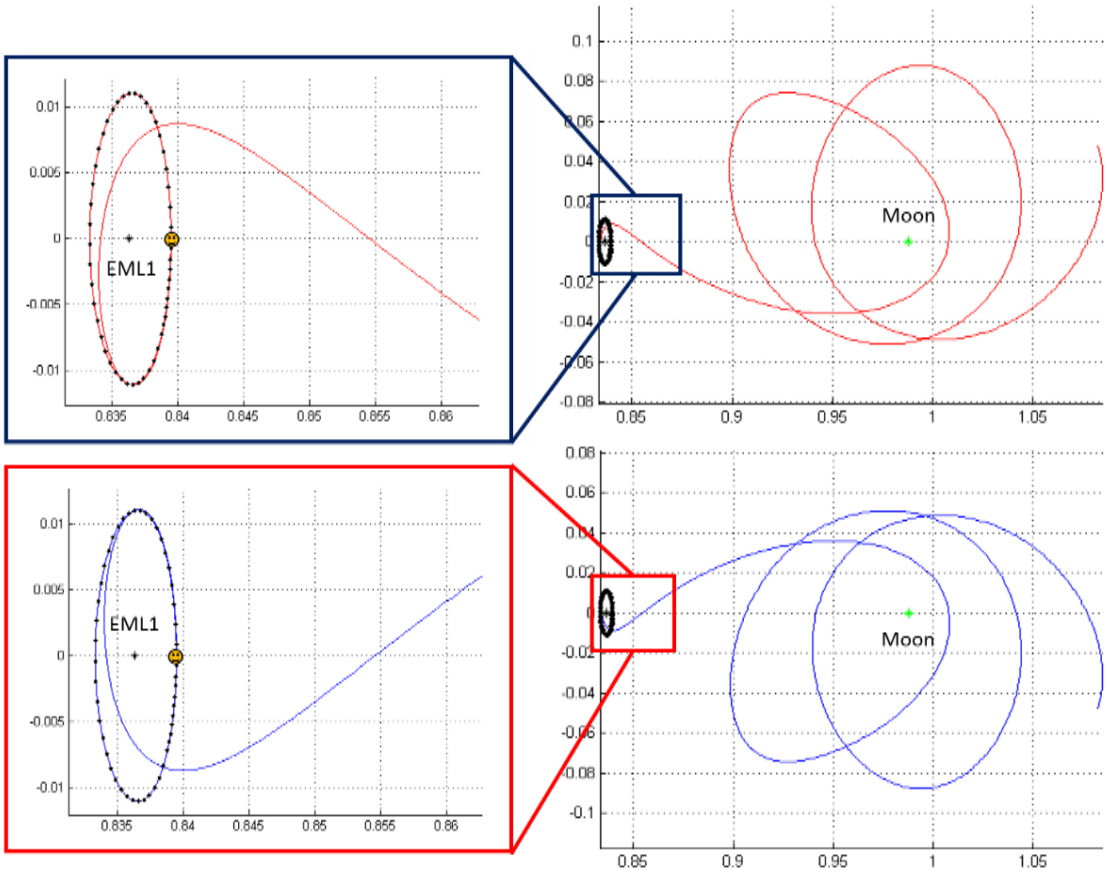

Figure 6. Initial one-dimensional trajectory from the periodic orbits around Earth-Moon L_1 point to unstable (red, top) and stable (blue, bottom) manifold direction

Table 2. Initial conditions for unstable and stable manifolds

	Initial Conditions
Unstable manifold to the exterior realm	$(\tilde{x} \quad y \quad v_x \quad v_y)_{t=0} = \alpha[1 \quad -\sigma \quad \lambda \quad -\lambda\sigma]$
Unstable manifold to the interior realm	$(\tilde{x} \quad y \quad v_x \quad v_y)_{t=0} = \alpha[-1 \quad \sigma \quad -\lambda \quad \lambda\sigma]$
Stable manifold to the exterior realm	$(\tilde{x} \quad y \quad v_x \quad v_y)_{t=0} = \alpha[1 \quad \sigma \quad \lambda \quad \lambda\sigma]$
Stable manifold to the interior realm	$(\tilde{x} \quad y \quad v_x \quad v_y)_{t=0} = \alpha[-1 \quad -\sigma \quad -\lambda \quad -\lambda\sigma]$

3.2 1-D Search Technique

Let us define the centerline of invariant manifolds as the limiting case where the tube width and the extent of the boundary Lyapunov orbit approach zero. In PCR3BP, one can express the equation of motion for m_3 in second-order differential equation form:

$$\ddot{x} - 2\dot{y} = \frac{\partial \bar{U}}{\partial x} \tag{3.2a}$$

$$\ddot{y} + 2\dot{x} = \frac{\partial \bar{U}}{\partial y} \tag{3.2b}$$

where $\bar{U} = \frac{1}{2}(x^2 + y^2) + \frac{1-\mu}{r_1} + \frac{\mu}{r_2}$, $r_1 = \sqrt{(x+\mu)^2 + y^2}$, $r_2 = \sqrt{(x-1+\mu)^2 + y^2}$.

3.2.1 Linearization in the Vicinity of L_1 and L_2 points

To describe the geometry of invariant manifolds in three-body dynamics, we can simply consider the equations of motion linearized near the equilibrium points. Consider that $x = x_L + \xi$, where x_L represents the L_1 or L_2 point, ξ is relatively small. Then we can express the equation of motion for m_3 in terms of ξ and y:

$$\ddot{\xi} - 2\dot{y} = \frac{\partial \bar{U}}{\partial x} \tag{3.3a}$$

$$\ddot{y} + 2\dot{x} = \frac{\partial \bar{U}}{\partial y} \tag{3.3b}$$

This can also be rewritten in the first-order form such that:

$$\dot{\xi} = v_x \tag{3.4a}$$

$$\dot{y} = v_y \tag{3.4b}$$

$$\dot{v_x} = 2v_y - \frac{\partial \bar{U}}{\partial \xi}(x_L + \xi, y) \tag{3.4c}$$

$$\dot{v_y} = -2v_x - \frac{\partial \bar{U}}{\partial y}(x_L + \xi, y) \tag{3.4d}$$

To linearize the above equations, the second-order partial derivative of the pseudo potential, U, can be calculated. Then we can expand $\frac{\partial \bar{U}}{\partial \xi}, \frac{\partial \bar{U}}{\partial y}$ about $\xi = 0, y = 0$.

Therefore the linearized first-order form of the equations of motion for PCR3BP become:

$$\dot{\xi} = v_x \tag{3.5a}$$

$$\dot{y} = v_y \tag{3.5b}$$

$$\dot{v_x} = 2v_y + ax \tag{3.5c}$$

$$\dot{v_y} = -2v_x - by \tag{3.5d}$$

where $a = -\left(\frac{\partial^2 \bar{U}}{\partial x^2}\right) = 1 + \frac{2(1-\mu)}{|x_L+\mu|^3} + \frac{2\mu}{|x_L-1+\mu|^3}, \quad b = -\left(\frac{\partial^2 \bar{U}}{\partial y^2}\right) = \frac{(1-\mu)}{|x_L+\mu|^3} + \frac{\mu}{|x_L-1+\mu|^3} - 1$. To simplify the equation, we can define a new term, $\bar{\mu}$:

$$\bar{\mu} = \frac{(1-\mu)}{|x_L+\mu|^3} + \frac{\mu}{|x_L-1+\mu|^3} \tag{3.6}$$

Then $a = 1 + 2\bar{\mu}, b = \bar{\mu} - 1$, $x = x_L + \tilde{x}$, and $\tilde{x} \ll r_h$. The energy integral E^* represents the energy surface that passes through the equilibrium points.

$$E^* = \frac{1}{2}\left({v_y}^2 + {v_y}^2 - ax^2 + by^2\right) \tag{3.7}$$

3.2.2 Geometry of Solutions with the Eigen State Analysis

The linearized equation of motion around the L_1 or L_2 points, the equation (3.5), can be represented in matrix form:

$$\frac{d}{dt}\begin{pmatrix}\tilde{x}\\ y\\ v_x\\ v_y\end{pmatrix}=\begin{bmatrix}0 & 0 & 1 & 0\\ 0 & 0 & 0 & 1\\ a & 0 & 0 & 2\\ 0 & -b & -2 & 0\end{bmatrix}\begin{pmatrix}\tilde{x}\\ y\\ v_x\\ v_y\end{pmatrix} \tag{3.8}$$

By adopting the Eigenvectors as the new coordinate system, we can better understand the geometry of the phase space. The Eigen state can be calculated straightforwardly from the above matrix forms, $\dot{X} = AX$.

When setting $\det(A - \lambda I) = 0$, the characteristic equation is found to be:

$$\lambda^4 + \lambda^2(2 - \bar{\mu}) + (1 + \bar{\mu} - 2\bar{\mu}^2) = 0 \tag{3.9}$$

Then the eigenvalue of the linearized equations are of the form $\pm\lambda$ and $\pm i\upsilon$.

$$\lambda_{1,2} = \pm\left[\frac{\bar{\mu}-2+\sqrt{9\bar{\mu}^2-8\bar{\mu}}}{2}\right]^{1/2} = \pm\lambda \tag{3.10a}$$

$$\lambda_{3,4} = \pm i\left[\frac{2-\bar{\mu}-\sqrt{9\bar{\mu}^2-8\bar{\mu}}}{2}\right]^{1/2} = \pm i\upsilon \tag{3.10b}$$

The eigenvectors, $\upsilon = (u_1, u_2, w_1, w_2)$ can be calculated from the relations with the eigenvalues: $A\upsilon = \lambda\upsilon$. The corresponding eigenvectors can be expressed in matrix form:

$$[u_1 \quad u_2 \quad w_1 \quad w_2] = \begin{bmatrix}1 & 1 & 1 & 1\\ -\sigma & \sigma & -i\tau & i\tau\\ \lambda & -\lambda & i\upsilon & -i\upsilon\\ -\lambda\sigma & -\lambda\sigma & \upsilon\tau & \upsilon\tau\end{bmatrix} \tag{3.11}$$

where $\sigma = \frac{2\lambda}{\lambda^2+b} > 0$, $\tau = -\left(\frac{\upsilon^2+a}{2\upsilon}\right) < 0$. Then the linearized equation of motion near the libration points can be expressed in the new coordinate system $(\xi, \eta, \zeta_1, \zeta_2)$:

$$\begin{pmatrix} \tilde{x} \\ y \\ v_x \\ v_y \end{pmatrix} = \begin{bmatrix} 1 & 1 & 1 & 1 \\ -\sigma & \sigma & -i\tau & i\tau \\ \lambda & -\lambda & iv & -iv \\ -\lambda\sigma & -\lambda\sigma & v\tau & v\tau \end{bmatrix} \begin{pmatrix} \xi \\ \eta \\ \zeta_1 \\ \zeta_2 \end{pmatrix} \tag{3.12}$$

In these Eigen state coordinates, the differential equation can simply described in new coordinate system $(\xi, \eta, \zeta_1, \zeta_2)$:

$$\dot{\xi} = \lambda\xi \tag{3.13a}$$

$$\dot{\eta} = -\lambda\eta \tag{3.13 b}$$

$$\dot{\zeta_1} = v\zeta_2 \tag{3.13 c}$$

$$\dot{\zeta_2} = -v\zeta_1 \tag{3.13d}$$

$$\mathrm{E} = \lambda\xi\eta + \frac{\upsilon}{2}\left({\zeta_1}^2 + {\zeta_2}^2\right) \tag{3.14}$$

The solution can be conveniently written as:

$$\begin{gathered} \xi(t) = \xi_0 e^{\lambda t} \\ \eta(t) = \eta_0 e^{-\lambda t} \\ \zeta_1(t) = \zeta_{10} cosvt + \zeta_{20} sinvt \\ \zeta_2(t) = \zeta_{20} cosvt - \zeta_{10} sinvt \end{gathered} \tag{3.15}$$

3.2.3 Centerline of Invariant Manifolds

The unstable manifolds winding around the Lyapunov orbits in L_1 or L_2 points would be in the form:

$$\begin{pmatrix} \xi \\ y \\ v_x \\ v_y \end{pmatrix} = \alpha e^{\lambda t} \begin{pmatrix} 1 \\ -\sigma \\ \lambda \\ -\lambda\sigma \end{pmatrix} + 2Re\left[\beta e^{ivt} \begin{pmatrix} 1 \\ -i\tau \\ iv \\ v\tau \end{pmatrix}\right] \tag{3.16}$$

Note that $|\beta|$ determines the radius of the manifold tube. By letting the radius approach zero, $|\beta| \to 0$, the exact solution for the initial conditions can be obtained. The

resulting one-dimensional path, called the centerline of the tube, implies the proper initial conditions needed for entry into the interior or exterior realm. These trajectories are the minimum energy paths within the tubes. The trajectory can be described in the linearized approximation:

$$\begin{pmatrix} \xi \\ y \\ v_x \\ v_y \end{pmatrix} = \alpha e^{\lambda t} \begin{pmatrix} 1 \\ -\sigma \\ \lambda \\ -\lambda\sigma \end{pmatrix} + H.O.T. \quad (\alpha > 0) \tag{3.17}$$

With these initial conditions, we can use the full nonlinear equation of motion to determine a centerline of the invariant manifolds. The equation of motion can be applied to calculate the centerline of tube as the solution for the second-order differential equations. Let us define new independent variable, $s \equiv e^{\lambda t}$. This can be easily expressed as:

$$\frac{d}{dt} = \frac{ds}{dt}\frac{d}{ds} = \frac{d}{dt}\left[e^{\lambda t}\right]\frac{d}{ds} = \lambda s \frac{d}{ds} \tag{3.18}$$

Then the equations of motion can be expressed in (ξ, y, v_x, v_y) coordinates with the new variable, s, as:

$$\frac{d\xi}{ds} = \frac{1}{\lambda s} v_x \tag{3.19a}$$

$$\frac{dy}{ds} = \frac{1}{\lambda s} v_y \tag{3.19b}$$

$$\frac{dv_x}{ds} = \frac{2}{\lambda s} v_y - \frac{1}{\lambda s}\frac{\partial \bar{U}}{\partial \xi}(x_L + \xi, y) \tag{3.19c}$$

$$\frac{dv_y}{ds} = -\frac{2}{\lambda s} v_x - \frac{1}{\lambda s}\frac{\partial \bar{U}}{\partial y}(x_L + \xi, y) \tag{3.19d}$$

Note that the initial condition can be obtained at s = 1.

$$\begin{pmatrix} \xi \\ y \\ v_x \\ v_y \end{pmatrix} = \alpha \begin{pmatrix} 1 \\ -\sigma \\ \lambda \\ -\lambda\sigma \end{pmatrix} \tag{3.20}$$

The above equations demonstrate the existence of the centerline in the invariant manifolds. To set up the initial condition summarized in Table 2, the centerlines of unstable and stable manifolds for both exterior and interior realms can be calculated.

3.2.4 Symmetries of Homoclinic and Heteroclinic Orbits

One of the important characteristics of invariant manifolds is the existence of the trajectories, called the homoclinic orbits, which are symmetric about the x-axis. The homoclinic orbits in both the interior and exterior realms was investigated by Conley (1968) and McGehee (1969) [16, 22]. Homoclinic orbits start from and return to the same Lagrange point, while Heteroclinic orbits connect two different Lagrange points. Through the heteroclinic orbits, which are linked with the invariant manifolds of the L_1 and L_2 Lyapunov orbits in the neck region, the homoclinic orbits in interior and exterior realms can be connected to each other. To examine the symmetry of the homoclinic orbits, let us bring back the equations of motion in the first-order form.

$$\dot{x} = v_x \tag{3.21a}$$

$$\dot{y} = v_y \tag{3.21b}$$

$$\dot{v_x} = 2v_y + x - \frac{2(1-\mu)(x+\mu)}{{r_1}^3} + \frac{2\mu(x-1+\mu)}{{r_2}^3} \tag{3.21c}$$

$$\dot{v_y} = -2v_x + y - \frac{(1-\mu)}{{r_1}^3} - \frac{\mu}{{r_2}^3} \tag{3.21d}$$

where $r_1 = \sqrt{(x+\mu)^2 + y^2}$ and $r_2 = \sqrt{(x-1+\mu)^2 + y^2}$.

To validate the symmetry on the x-axis, we can transform the variables: $\tilde{y} = -y$ and $\hat{t} = -t$. Then the equation of motion can be represented as:

$$\frac{dx}{d\tilde{t}} = -v_x \tag{3.22a}$$

$$\frac{d\tilde{y}}{d\tilde{t}} = v_y \tag{3.22b}$$

$$\frac{dv_x}{d\tilde{t}} = -\left(2v_y + x - \frac{2(1-\mu)(x+\mu)}{{r_1}^3} + \frac{2\mu(x-1+\mu)}{{r_2}^3}\right) \tag{3.22c}$$

$$\frac{dv_y}{d\tilde{t}} = -\left(-2v_x - \tilde{y} + \frac{(1-\mu)}{{r_1}^3}\tilde{y} + \frac{\mu}{{r_2}^3}\tilde{y}\right) \tag{3.22d}$$

where $r_1 = \sqrt{(x+\mu)^2 + \tilde{y}^2}$ and $r_2 = \sqrt{(x-1+\mu)^2 + \tilde{y}^2}$. When we assume that $\tilde{v}_x = -v_x$, the equations (3.22) match exactly with the equations (3.21). Hence, the equations (3.22) with initial conditions, $\left(x_0, -y_0, -v_{x_0}, v_{y_0}\right)$, are a mirror image of the trajectory which is generated by the equations (3.21) with initial conditions, $\left(x_0, y_0, v_{x_0}, v_{y_0}\right)$. Expressed in the x-y plane, this homoclinic orbit shows the symmetry about the x-axis. In a similar manner, the heteroclinic orbits associated with the L_1 and L_2 Lyapunov orbits are approximately symmetric about the y-axis with small μ.

By combining the symmetric homoclinic and heteroclinic orbits, the interior and exterior realms of the PCR3BP can be connected. Therefore, using the centerline of the invariant manifolds and their symmetries, a sequence of one-dimensional searches allows us to design the trajectory around the Lagrange points.

3.3 Preliminary Design for NEA Rendezvous Mission

As one of the 1-D search technique applications, Near-Earth Asteroids (NEAs) rendezvous mission design is considered. Since NEAs continually pose a threat to the safety of Earth, NEAs exploration and mitigation are crucial tasks for defending our planet. There is also a huge possibility of extracting valuable materials from asteroids. They have many valuable resources that can be brought back to Earth or used in space for spacecraft propulsion systems or space habitations. To find fuel-optimized trajectories to NEAs, the IPSH method is fully exploited to transfer from the Earth-Moon system to the Sun-Earth system. As in Figure 7, the overall mission trajectory is divided into four phases: Phase 1) LEO orbit to the Lyapunov orbit around Earth-Moon L_1 point; Phase 2) Earth-Moon L_1 Lyapunov orbit to Earth-Moon L_2 point; Phase 3) Earth-Moon L_2 point to Sun-Earth L_2 point; and Phase 4) Sun-Earth L_2 point to NEA.

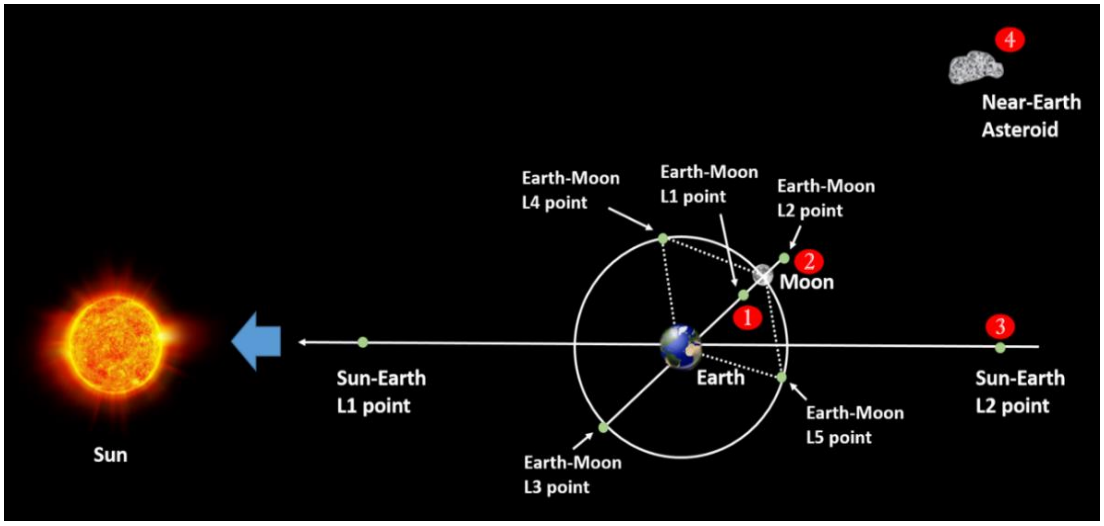

Figure 7. Asteroid rendezvous mission trajectory

Computationally, it is more convenient to generate the symmetric heteroclinic orbit between Lyapunov orbit in Earth-Moon L_1 point and Earth-Moon L_2 point in the neck region. Therefore we started in the neck region of the Earth-Moon system to generate the trajectory of phase 2 first by integrating the equations in reverse time and starting from the Earth-Moon L_2 point stable manifold. A 1 metric ton (1MT) spacecraft using ion engines with the specific impulse, I_{sp} = 3000 s, can take the centerline of unstable manifolds to the interior realm at the Earth-Moon L_2 point using negligible thrust. Note that the appropriate initial perturbations for the unstable manifolds to the interior realm are used from Table 2. Then, as seen in Figure 8, the S/C encircles the Moon twice and then reaches to the Earth-Moon L_1 point in 43.7 days. To obtain the outward bound trajectory, we simply start at the Earth-Moon L_1 Lyapunov orbit and integrate in forward time.

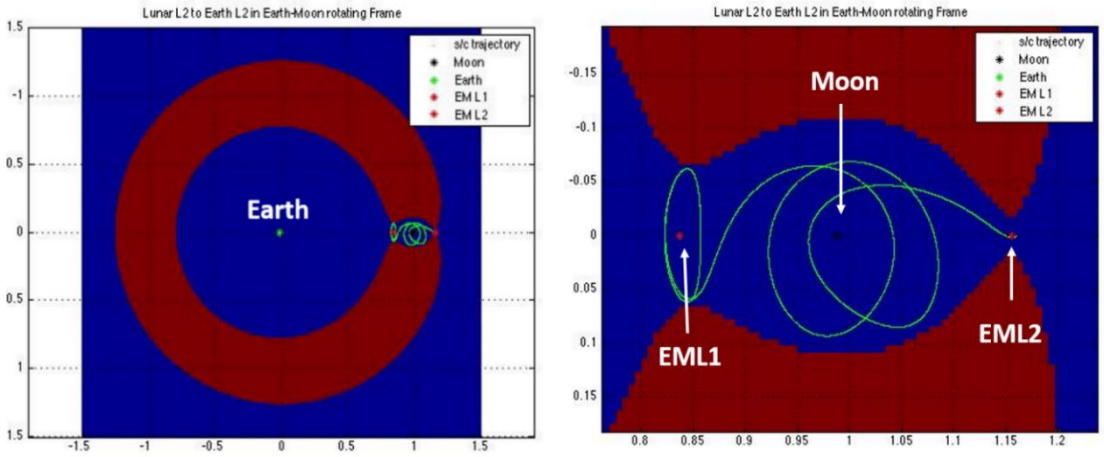

Figure 8. Phase 2 from Earth-Moon L_1 periodic orbit to Earth-Moon L_2 point

When the S/C reaches the Lyapunov orbit of the Earth-Moon L_1 point, the trajectory to Earth (LEO/GEO) can be generated in reverse time. The Earth-Moon L_1 point has been chosen as a connecting place for phase 1 because it results in the maximum number of opportunities to take on supplies, exchange crew or deal with emergencies. With the initial conditions for stable manifolds to the interior realm at the Earth-Moon L_1 periodic orbit, the S/C slowly spirals back into the Earth. As seen in Figure 9, a small amount (0.24 N) of kick-start thrust is necessary for 4.2 months, consuming 96 kg of fuel. The total trip time is 156 days (5.2 months), which is longer than the traditional transfer methods like Hohmann Transfer, but the total ΔV is significantly reduced to 2.698 km/s. Through the Lyapunov orbit in Earth-Moon L_1 point, which is the crucial link between phase 1 and phase 2, the S/C can travel from the interior realm to the exterior realm of the Earth-Moon system.

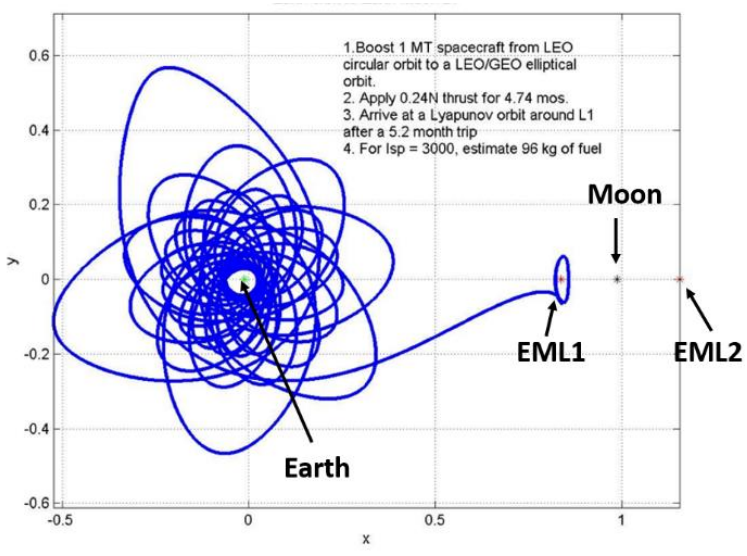

Figure 9. Phase 1 from LEO to Earth-Moon L_1 periodic orbit

3.3.1 4-Body Dynamics for Coupled Two 3-Body Systems

Now we can proceed to investigate the trajectory of phase 3, which is to connect from the Earth-Moon L_2 point to the Sun-Earth L_2 point. To consider the transfer trajectory from the Earth-Moon system to the Sun-Earth system, the four-body dynamics are implemented as two coupled three-body problems [1]. The four bodies, Sun-Earth-Moon-S/C, can be split in two perturbed three-body problems as Sun-Earth-Spacecraft (CCM) perturbed by the Moon and Earth-Moon-Spacecraft (BCM) perturbed by the Sun. The geometry of the four-body problem [1] is illustrated in Figure 10. The equations of motion for this four-body problem can be described as:

$$\dot{x} = u \tag{3.23a}$$

$$\dot{y} = v \tag{3.23b}$$

$$\dot{u} = x + 2v - C_E(x + \mu_M) - C_E(x - \mu_E) - C_s(x - x_S) - \alpha_S x_S \tag{3.23c}$$

$$\dot{v} = y - 2u - C_E y - C_M y - C_s(y - y_S) - \alpha_S y_S \tag{3.23d}$$

where $C_i = \frac{\mu_i}{{r_i}^3}$ $for\ i = E, M, S$, $\alpha_S = \frac{m_S}{{\alpha_S}^3}$.

In Figure 11, the thrust-free trajectory obtained via a one-dimensional search of the correct phasing of the Earth-Moon L_2 departure is shown in the Earth-Moon rotating frame (left) and the Sun-Earth rotating frame (right). For 39.4 days, the S/C travels the immense distance from unstable manifolds to the exterior realm without fuel expenditure.

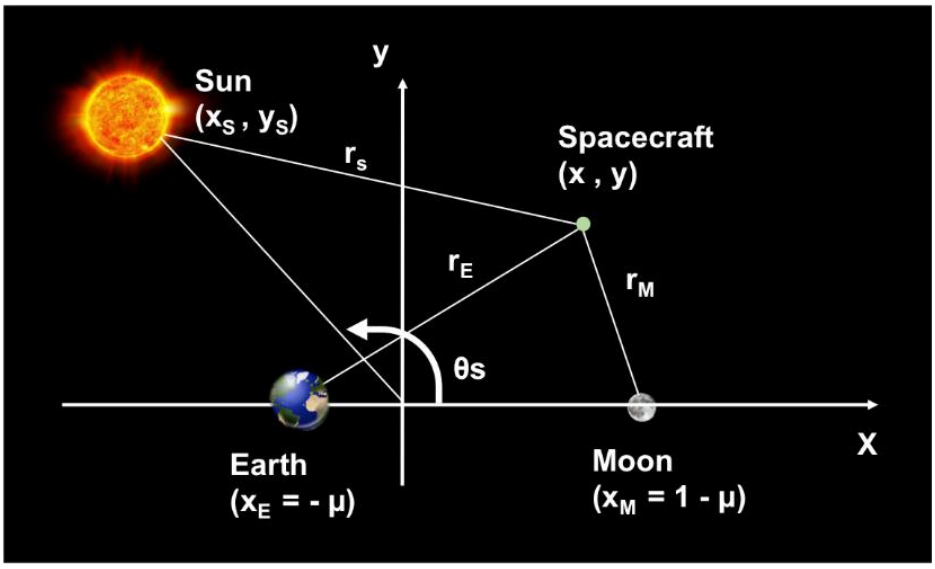

Figure 10. Geometry of the four-body problem (Sun-Earth-Moon-Spacecraft)

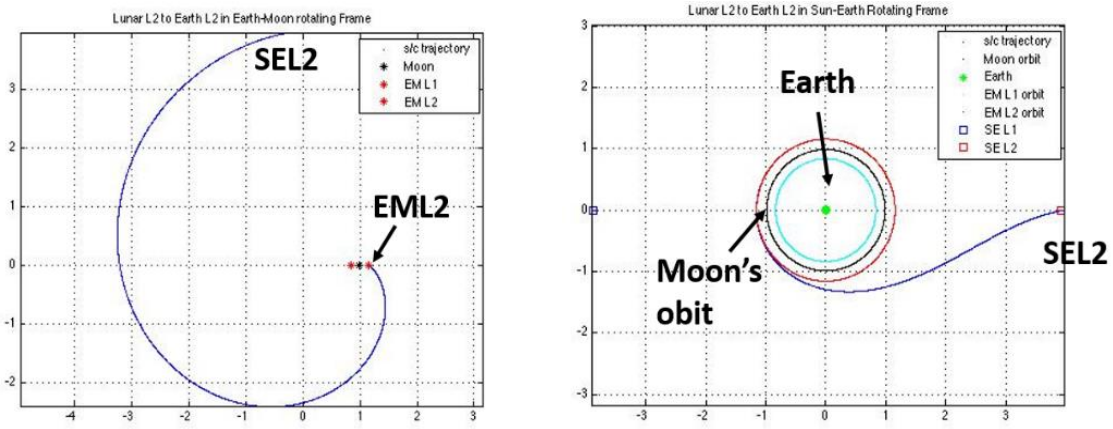

Figure 11. Phase 3 from Earth-Moon L_2 point to Sun-Earth L_2 point in Earth-Moon rotating frame (left) and in Sun-Earth rotating frame (right)

Phase 4 is the trajectory, called the Grand Tour [23, 24], from the Sun-Earth L_2 point via Near-Earth Asteroids which visit both regions that are ~0.15 AU below and above the Earth's orbit, and then back to the original point. During the segment of the

trajectory indicated by the red line in Figure 12, the S/C departs from Sun-Earth L_2 point through the unstable manifold to the exterior realm direction by executing a small thrust, 0.264N for 138 days. The small increment of the thrust changes the energy state of the system so that the neck region of the forbidden zone opens outward as you can see in Figure 13. Therefore the S/C can enter the internal region of the Sun-Earth system. By passing through the interior realm, the S/C coasts along the blue line in Figure 12. When it approached to the wall of forbidden zone, the S/C can be pushed in the opposite direction with a second small thrust, 0.264N for another 138 days. Finally, it can travel the unpowered return trajectory in the exterior realm (sky-blue line) and back to the Sun-Earth L_2 point. During this 9.2 months grand tour to reach NEAs, the total ΔV is 5.708 km/s which consumes 214.06 kg of fuel mass. The summary of total trip time and ΔV is shown in Table 3.

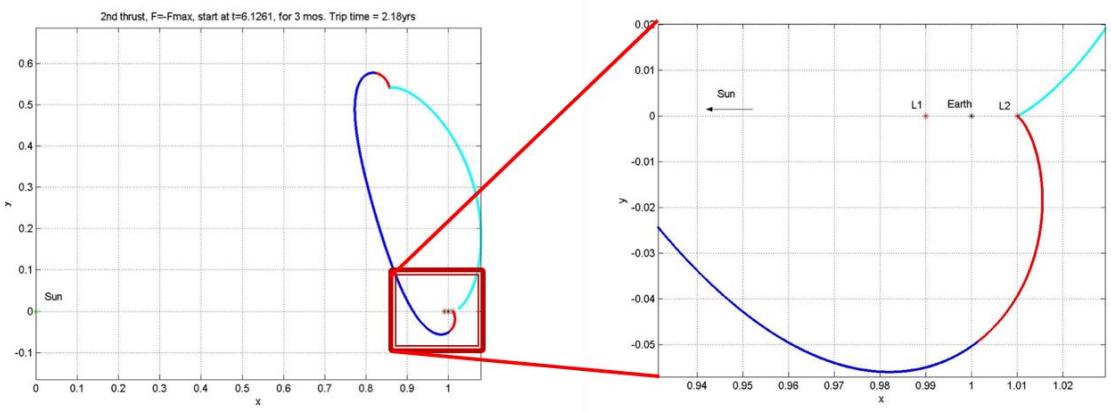

Figure 12. Asteroid rendezvous mission trajectory: phase 4 grand tour

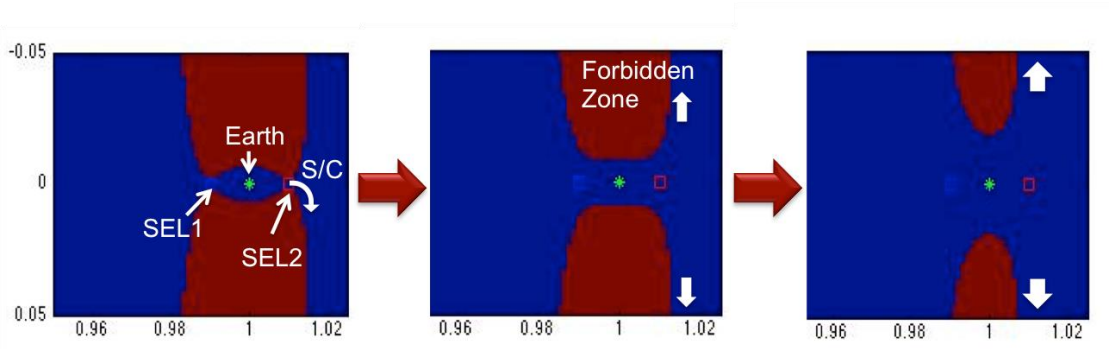

Figure 13. Transformation of forbidden zone around neck region by increasing energy state

Table 3. Summary of cost for NEAs rendezvous mission

	TOF [days]	**ΔV [km/s]**
Phase 1: LEO to Earth-Moon L1	156	2.698
Phase 2: Earth-Moon L1 to L2	43.7	0
Phase 3: Earth-Moon L2 to Sun-Earth L2	39.4	0
Phase 4: Grand Tour	604.5	5.708
Total	843.6 (=2.3 yrs)	8.406

4. DESIGN TRAJECTORY FROM EARTH TO MARS

By using the low-energy trajectory method, ISPH, a novel design of a solar sail mission for Mars exploration can be developed. Invariant manifolds, which are winding around the Lagrangian points, can be helpful to transfer a spacecraft with almost no fuel consumption. This energy efficient method makes Mars exploration mission more attainable. Moreover, the topology of invariant manifolds can be transformed by deploying solar sails. Solar sails provide a propulsive power using solar radiation pressure. Assuming the sail is isotropic, that is, it produces a radiation force equivalent to a spherical reflector, and the effect of the solar sail on the system dynamics is to modify the gravitational constant of the Sun, while the centrifugal force in the rotating frame remains the same. Therefore, the Sun-Mars L_1 and L_2 Lagrangian points will be shifted toward the Sun and the geometry of the invariant manifolds around L_1 and L_2 points will be changed. By taking advantage of these features, a low-thrust trajectory for Mars exploration is developed.

The PCR3BP will be considered since Earth and Mars are nearly co-planar planets. The first stage is the trajectory from Earth to Sun-Earth L_2 point. When the spacecraft reaches Sun-Earth L_2 point, the solar sail can be launched with a slight nudge into the invariant manifold leading to the exterior realm. At this second stage, the spacecraft leaves the neck regions and obtains an extra acceleration from the solar radiation pressure force. Meantime the centrifugal force, Fc has to be conserved for the three bodies. Let define a factor, $f = (F_{m1})_{final}/(F_{m1})_{initial}$, where F_{m1} is the Sun's

gravitational force and $f = 1$ means no solar sail effect as an initial state. When f becomes close to zero, Sun's gravitational force will be cancelled by increasing the solar radiation pressure force, F_{SRP}. The acceleration depends on the reflectivity of the solar sail material and also its size. Assume that the solar sail is large enough to cancel Sun's gravitational force by solar pressure here. Then the Sun-Mars Lagrangian points move toward the Sun as f becomes smaller. Also the configuration of invariant manifolds for Sun-Mars system will be changed along with the Lagrangian points. Here we can get an advantage by reducing the distances of the L_1 and L_2 points from the Sun. It means that the positions of the Sun-Mars L_1 and L_2 points can be closer to the spacecraft, which is near Sun-Earth L_2 point. At the last stage, the spacecraft can transfer to the approached Sun-Mars L_1 point with a small thrust.

4.1 Investigation for Omni-directional Solar Sail Power

Consider a spacecraft moving around under the massive m_1 and m_2 gravitational fields. Assume that the three bodies are in the same plane and that m_1 and m_2 are around in a circular orbit about their center of mass. The equations of motion for the three-body problem can be described as:

$$m_1\ddot{x_1} = \frac{-Gm_1m_2}{|x_1-x_2|^3}(x_1 - x_2) \tag{4.1a}$$

$$m_2\ddot{x_2} = \frac{Gm_1m_2}{|x_1-x_2|^3}(x_1 - x_2) \tag{4.1b}$$

$$m\ddot{x} = f\frac{Gm_1m}{|x-x_2|^3}(x_1 - x) + \frac{Gm_2m}{|x-x_2|^3}(x_2 - x) + F \tag{4.1c}$$

where the solar sail factor is $f = (F_{m1})_{final}/(F_{m1})_{initial}$, which will affect the equations of motion only for m_1, F_{m1} is the Sun's gravity force, and F is an additional thrust. Alternatively the equations of motion can be written as:

$$\ddot{x} - 2\dot{y} = -\frac{\partial \bar{U}}{\partial x} \tag{4.2a}$$

$$\ddot{y} + 2\dot{x} = -\frac{\partial \bar{U}}{\partial y} \tag{4.2b}$$

where the effective potential $\bar{U} = -\frac{1}{2}(x^2 + y^2) - f\frac{1-\mu}{r_1} - \frac{\mu}{r_2}$; $r_1 = \sqrt{(x+\mu)^2 + y^2}$; $r_2 = \sqrt{(x-1+\mu)^2 + y^2}$. For the advanced approach to describe the motion of this Sun-Mars system, the four body dynamics of Sun, Earth, Mars, and spacecraft can be considered later. To calculate L_1 and L_2 positions, the equilibrium points need to be solved. The PCR3BP allows five equilibrium point solutions, which are including the collinear equilibria on the x-axis (y=0) L_1, and L_2.

For L_1 and $x < (1-\mu)$: $$f\frac{(1-\mu)}{(x+\mu)^2} - \frac{\mu}{(x-1+\mu)^2} - x = 0 \tag{4.3a}$$

For L_2 and $x > (1-\mu), (x-1+\mu) > 0$: $$f\frac{(1-\mu)}{(x+\mu)^2} + \frac{\mu}{(x-1+\mu)^2} - x = 0 \tag{4.3b}$$

By using $x = \delta + 1 - \mu$, the equations can be expressed in δ. Equation (4.3) defines recursive sequences obtained by successive substitution of δ into the right hand side. The infinite sequences are convergent.

$$L_1: \delta = -\left(\frac{\mu(1+\delta)^2 + (1-\mu)\delta^2(1-f+\delta^2)}{(1+\delta)^2 + 2(1-\mu)}\right)^{1/3} \tag{4.4a}$$

$$L_2: \quad \delta = \sqrt{\frac{(\mu-\delta^3)}{(1-\mu)} + f\frac{\delta^2}{(1+\delta)^2}} \tag{4.4b}$$

As seen in Figure 14, both the distances of Sun-Mars L_1 and L_2 points from the Sun decrease from their initial state by reducing the solar sail factor *f*. It means that the Sun-Mars L_1 and L_2 points can shift toward the Sun. The factor *f* can be changed by the solar sail effect, dragging the Sun-Mars L_1 point near the spacecraft that is around the Sun-Earth L_2 point. It is like docking the spacecraft over the Sun-Mars L_1 point. The configuration of the invariant manifolds around the Sun-Mars L_1 and L_2 points will be transformed, since it is formed with Lyapunov orbit around the L_1 and L_2 points. Therefore, the Sun-Mars L_1 point can meet the Sun-Earth L_2 point around $f = 0.291$. The forbidden zone, which is inaccessible for a given energy, and its neck region are shown in Figure 15.

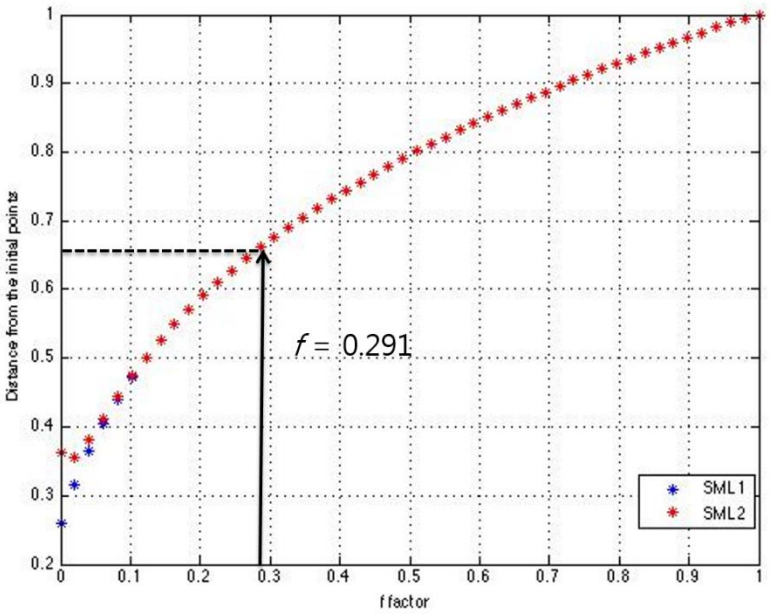

Figure 14. Sun-Mars L_1 and L_2 points change by reducing *f*

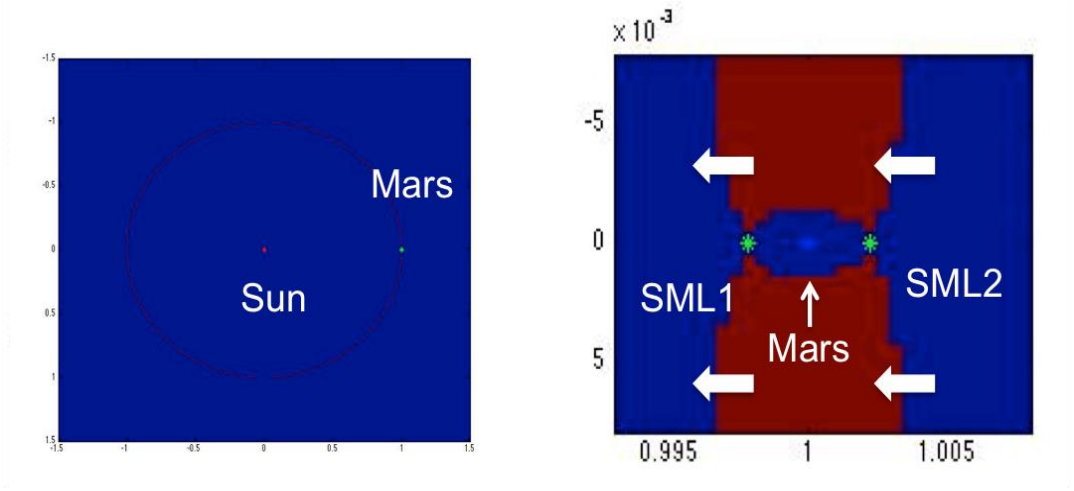

Figure 15. Sun-Mars L_1 and L_2 points shifting toward to Sun by reducing *f*

The change of the invariant manifold structure in the four-body system by reducing *f* will be studied in a geometrical view. This framework of tube dynamics leads us to find intersected regions between Sun-Earth manifolds systems and the Sun-Mars system. Based on the previous research done by German and Frabcesco [25-27], two circular restricted three-body systems with similar mass parameters cannot approach one another even in developing the manifolds for a long integration time. Therefore various researchers designed the transfer trajectory from one system to another combining with the traditional differential correction method, or shooting method. However, the system-to-system trajectory design directly through manifolds can possibly be done by this research with solar sail effect. We will explore the limited case of 4-body problem and design advanced transfer trajectories with significantly reduced ΔV compared with previous work.

4.2 Limited Case of 4-Body Problem

Consider a simple case of a 4 body problem with Sun-Earth-Mars-S/C system. It can be divided into two 3-body models with specific assumptions. First, the two components of the models are the planar circular restricted 3-body problems with Sun-Earth-S/C systems and Sun-Mars-S/C systems. Second, the Sun is at the origin of the 4-body problem. In this case, the circular orbits of the Earth and Mars are described proportionally with their semi-major axes and orbital periods. These assumptions have a limit of mathematical precision with errors of the order of μ since μ has different values for each case of Earth and Mars. However, the difference is small enough (less than $3x10^{-6}$) to be ignored. Simply using these assumptions to the limited case of 4-body model, a basic tractable formulation can be developed. This can be a guideline of 4-body dynamics to enhance understanding of the mathematical and geometrical framework to describe the modification of the structure for the 4-body system due to the effects of the solar sail. The results show that system-to-system transfer trajectories can be designed by changing the configuration of the invariant manifolds.

4.2.1 Equations of Motion for the Limited Case of 4 Body Problem

Assume the Sun is at the origin when the Earth and Mars are on their circular orbits. To describe this limited 4-body problem in the Sun-Earth rotating frame, let us define the dimensionless quantities for position x, time t, mass parameter μ.

$$x = \frac{\tilde{x}}{|\widetilde{r_E}|} \tag{4.5}$$

where $\tilde{x}$ is the position vector of S/C and $\widetilde{r_E}$ is the position vectors of Earth.

$$t = \tilde{t}\Omega \tag{4.6}$$

where $\tilde{t}$ is time and Ω is angular velocity of Sun-Earth rotating frame, $\Omega = \sqrt{\frac{m_s G}{|r_E|^3}}$

$$\mu_E = \frac{m_E}{m_S}, \quad \mu_M = \frac{m_M}{m_S} \tag{4.7}$$

Where m_S, m_E, m_M are the mass of the Sun, Earth and Mars respectively. Note that μ_E and μ_M are the mass parameters for the Sun-Earth system and the Sun-Mars system. Since the distance between the Sun and the Earth is set to unity, the relative position and angular velocity of Mars can be calculated in the Sun-Earth rotating frame.

$$r = \frac{|\widetilde{r_M}|}{|\widetilde{r_E}|} = 1.5235 \tag{4.8}$$

$$\omega_M = 1 - \frac{T_M}{T_E} = 0.5317 \tag{4.9}$$

where $\widetilde{r_M}$ is the position vectors of Mars, ω_M is angular velocity of Mars, T_E and T_M are the orbital periods of the Earth and Mars, respectively. With these dimensionless components, the equations of motion of the limited 4-body problem can be expressed in x-y plane.

$$\ddot{x} = 2\dot{y} + x - f\frac{x}{R^3} + \mu_E\frac{(1-x)}{{R_E}^3} + \mu_M\frac{(r_x-x)}{{R_M}^3} + F_x \tag{4.10a}$$

$$\ddot{y} = -2\dot{x} + y - f\frac{y}{R^3} + \mu_E\frac{y}{{R_E}^3} + \mu_M\frac{(r_y-y)}{{R_M}^3} + F_y \tag{4.10b}$$

where R, R_E, R_M are the distances between the Sun and S/C, Earth, and Mars, respectively: $R = \sqrt{x^2+y^2}, R_E = \sqrt{(1-x)^2+y^2}, R_M = \sqrt{(r_x-x)^2+(r_y-y)^2}$. The position of Mars can be described in terms of r_x and r_y: $r_x = rcos(-\omega_M t + \varphi_0), : r_y = rsin(-\omega_M t + \varphi_0)$ with φ_0 is the initial phase angle of Mars. The factor by which the solar sail decreases the solar gravitational parameter is denoted by *f*. The external force

divided by the S/C mass is expressed in two components, F_x and F_y. In Figure 16, the geometry of 4-body systems is shown.

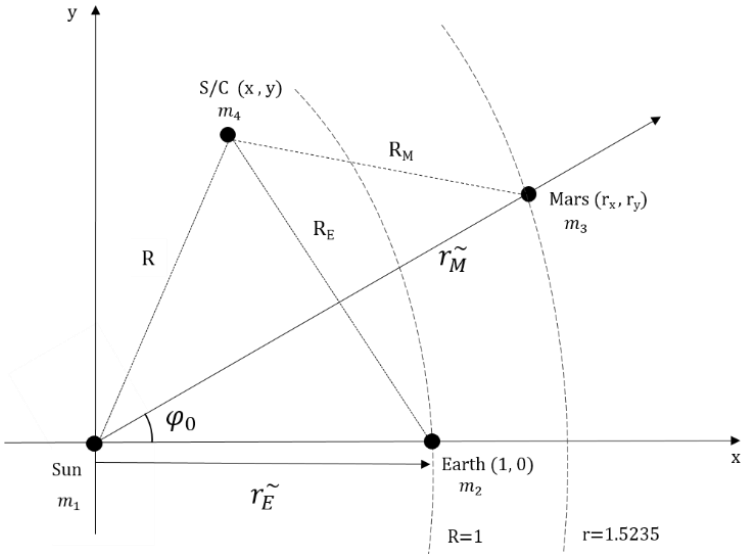

Figure 16. Geometry of the limited 4-body problem

Let us investigate the existence of the force-free Lagrange points, ${x_E}^*$, ${x_M}^*$ in the limited 4-body problem. For the Sun-Earth system, the Sun-Earth Lagrange points can be calculated when $\mu_M = 0$.

$$ {x_E}^* = 1 + \delta \tag{4.11a} $$

For L_1: $$ \delta \leftarrow -\left(\frac{1}{3}[\mu_E(1+\delta)^2 + 3\delta^4 + \delta^5 + \delta^2]\right)^3 \tag{4.11b} $$

For L_2: $$ \delta \leftarrow \sqrt{\mu_E + f\frac{\delta^2}{(1+\delta)^2} - \delta^3} \tag{4.11c} $$

To get the distance from the origin of the Sun-Mars Lagrange points, solve δ after replacing μ_E by μ_M in the equation (4.11).

$$x_M{}^* = r(1+\delta) \tag{4.12a}$$

For L_1: $$\delta \leftarrow -\left(\frac{1}{3}[\mu_M(1+\delta)^2 + 3\delta^4 + \delta^5 + \delta^2]\right)^3 \tag{4.12b}$$

For L_2: $$\delta \leftarrow \sqrt{\mu_M + f\frac{\delta^2}{(1+\delta)^2} - \delta^3} \tag{4.12c}$$

Note that the x-y position of the Sun-Mars L_1 and L_2 points can be expressed in the Sun-Earth rotating frame.

$$(x_M{}^*)_{SE} = x_M{}^* \cos(-\omega_M t + \varphi_0) \tag{4.13a}$$

$$(y_M{}^*)_{SE} = y_M{}^* \sin(-\omega_M t + \varphi_0) \tag{4.13a}$$

For the example trajectory, we can assume that the initial phase angle of Mars is $\varphi_0 = 4.4139 = 252.9^\circ$. The mission scenario is: First, the solar sail is deployed at the Sun-Earth L_2 point and embarks onto the unstable manifolds to the exterior realm. Second, the value of the solar sail factor, *f* is decreased in proportion to the mission time starting from *f* = 1 to 0.83. By applying those conditions to the equation of motion (4.10), the trajectory from the Sun-Earth L_2 point to the vicinity of the Sun-Mars L_1 point can be obtained. The trajectories in the Sun-Earth and Sun-Mars rotating frame are shown in Figures 17 and 18. As the factor *f* is changed, both the Sun-Earth and Sun-Mars Lagrange points are shifted toward to the Sun. Since the factor *f* is decreased discretely in three steps from 1 to 0.83, discontinuous points in the motions of Sun-Earth L_1 and L_2 points can be found in Figure 18. Interestingly, there is a bounce back motion of S/C trajectory in the vicinity of the Sun-Mars L_1 point. In Figure 19, the Sun-Mars L_1 point is moved toward to the Sun while the factor *f* is decreased. Then the S/C penetrates a little beyond the Sun-Mars L_1 point but turns back to the interior realm of the Sun-

Mars system again. It is necessary to investigate the energy state and the eigen state analysis of this resulting motion with the factor *f*.

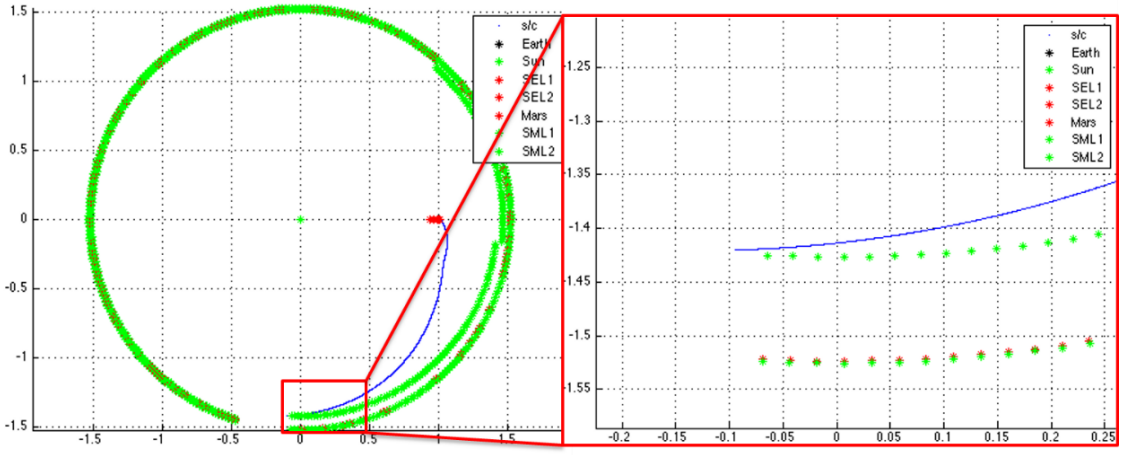

Figure 17. S/C trajectory from the Sun-Earth L_2 point to the vicinity of the Sun-Mars L_1 point in the Sun-Earth rotating frame

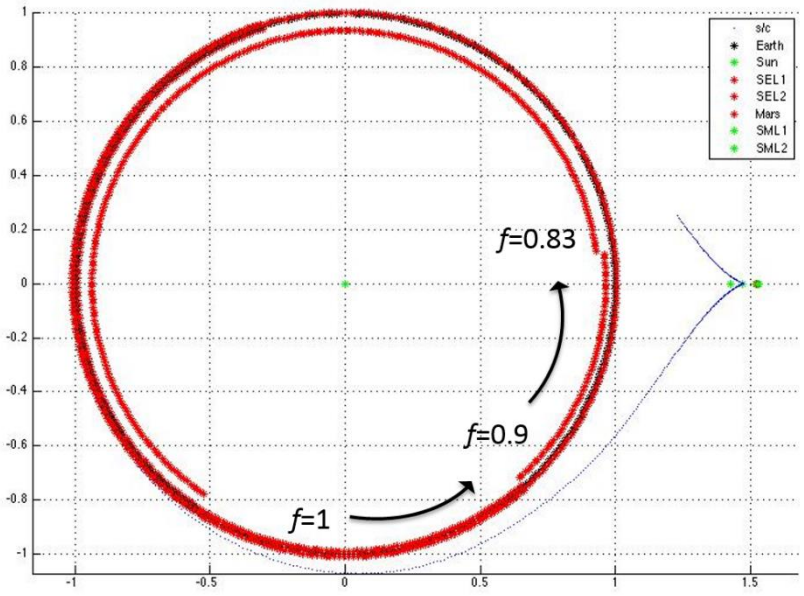

Figure 18. S/C trajectory from the Sun-Earth L_2 point to the vicinity of the Sun-Mars L_1 point in the Sun-Mars rotating frame

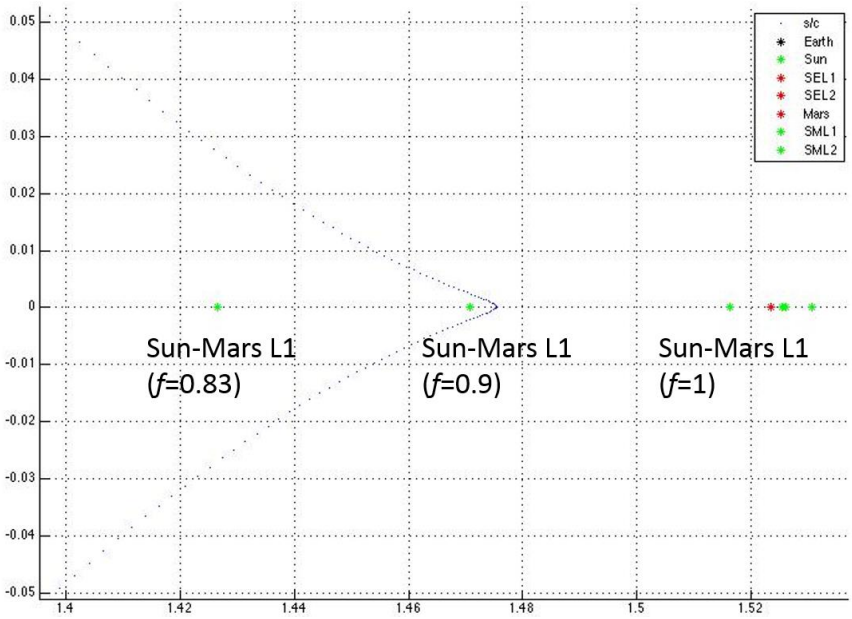

Figure 19. Close up of the trajectory near the Sun-Mars L_1 point in the Sun-Mars rotating frame

4.2.2 Energy State and Eigen State for the Limited Case of 4-Body Problem

To understand the bounce back motion with decreasing *f*, let us explore the geometry of the system near the neck region. The energy integral for the Sun-Earth-S/C system in the Sun-Earth rotating frame can be expressed in:

$$E_{SE} = \frac{1}{2}\left(v_x{}^2 + v_y{}^2\right) - \frac{1}{2}(x^2 + y^2) - \frac{f}{R} - \frac{\mu_E}{R_E} \tag{4.14}$$

The spacecraft can move around the interior and exterior realms through the neck region near the L_1 and L_2 points when the energy level of the system is between E_2 and E_3. It is this case 3 ($E_2 \leq E \leq E_3$) which is one of the typical energy regimes of the PCR3BP (See Figure 4). Let us take the value of E_{SE} = -1.50045 while the factor *f* is 1. This value of the energy is just enough to open the neck regions slightly as seen in

Figure 20. However if we put f = 0.83 and use E_{SE} = -1.32482 to maintain the neck region open, the forbidden zone is entirely shifted to the left side of the Earth in Figure 21. It means that the energy state of the system can be affected by changing the value of the factor f.

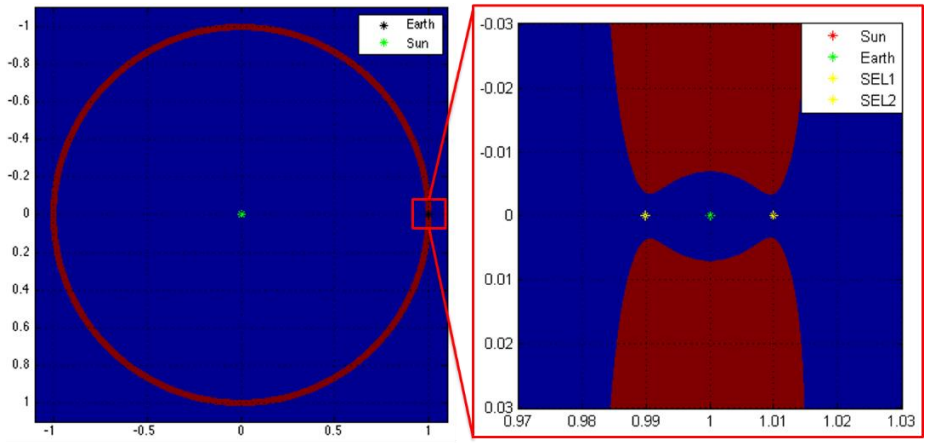

Figure 20. Forbidden zone for the Sun-Earth-S/C system in the Sun-Earth rotating frame when f = 1 and E_{SE} = -1.50045

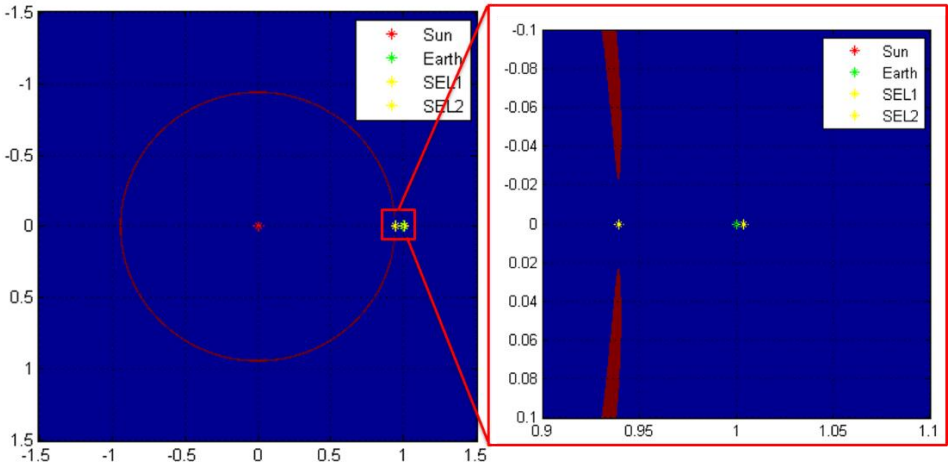

Figure 21. Forbidden zone for the Sun-Earth-S/C system in the Sun-Earth rotating frame when f = 0.83 and E_{SE} = -1.32482

To investigate the relationship between the energy integral and the solar sail factor *f*, we can fix one parameter and change the other one. In Figure 22, the factor *f* is decreased from 1 to 0.9991 while the value of energy is set to E_{SE} = -1.50045. The neck region with two throats is closed so that the S/C cannot move from the interior to the exterior realm. Also the thickness of the forbidden zone is increased when the factor *f* is decreased. It means that the required energy limit to maintain the neck region open in the energy state phase is increased by reducing the solar sail factor *f*. In Figure 23, the energy E_{SE} is increased from -1.50045 to -1.50001 while the factor *f* is kept at1. Then the forbidden zone becomes thinner and is shifted to the left slightly while the neck region opens widely upwards. The two throats of the neck region are reduced to one throat at E_{SE} = -1.50001 and then entirely disappear when E_{SE} is larger than -1.3. Therefore 1) the critical limits of the energy level to open the neck region are increased while the factor *f* is decreased and 2) the entire forbidden zone is shifted slightly toward the Sun's direction while E_{SE} is increased. In Figure 24, the forbidden zone can keep a neck region open by increasing the energy E_{SE} over the critical limits while the solar sail factor *f* is decreasing.

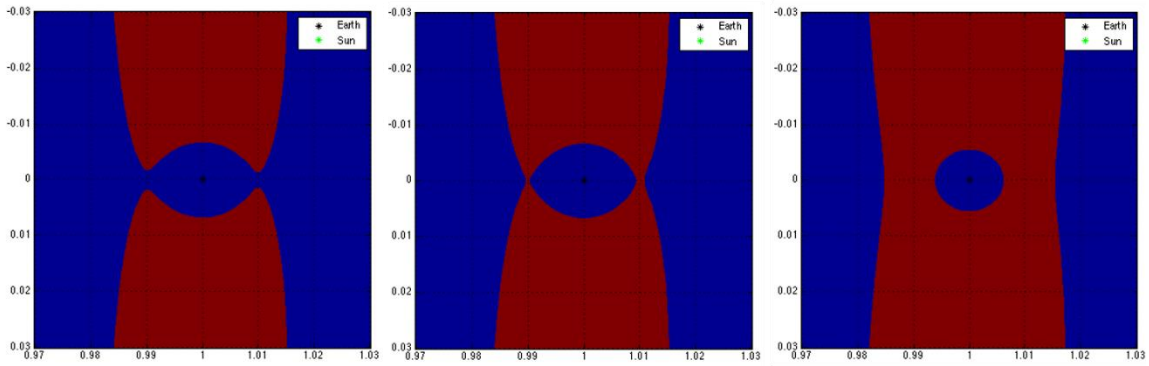

Figure 22. Forbidden zones when *f* is decreasing with fixed energy E_{SE} = -1.50045 (*f* = 1 (left), *f* = 0.9999 (middle), *f* = 0.9991 (right))

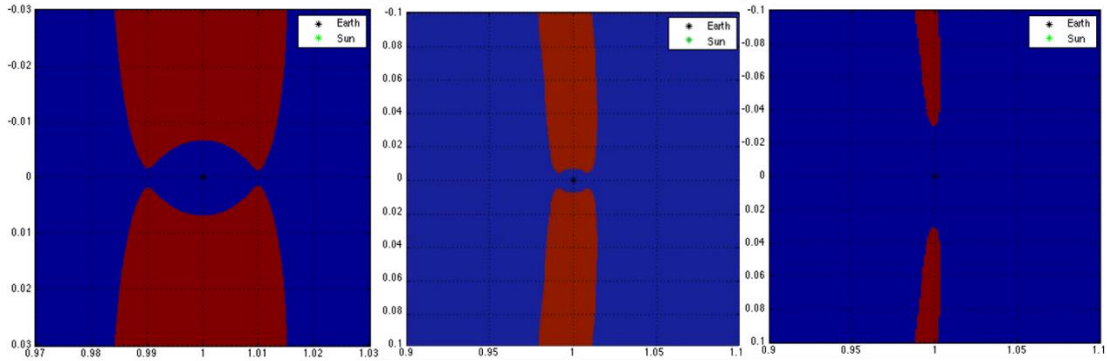

Figure 23. Forbidden zones when E_{SE} is increasing with fixed *f* = 1 (E_{SE} = -1.50045 (left), E_{SE} = -1.50023 (middle), E_{SE} = -1.50001 (right))

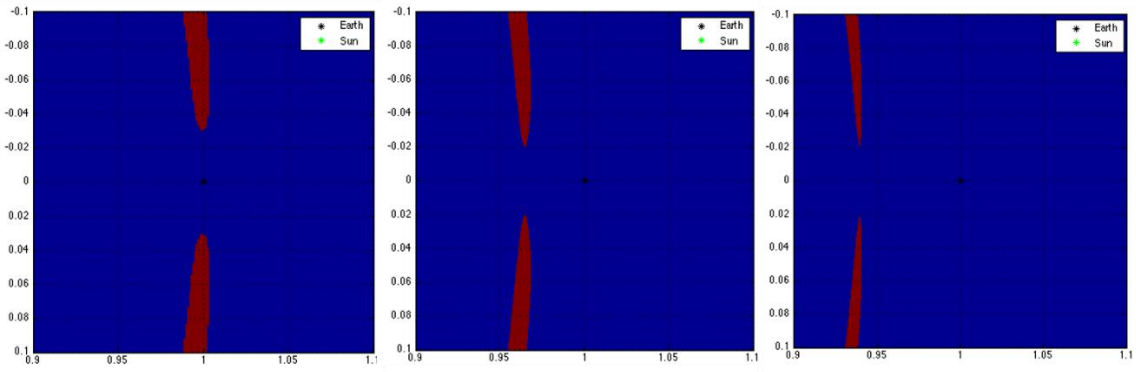

Figure 24. Forbidden zones with different *f* and energy E_{SE} (*f* = 1, E_{SE} = -1.5001 (left), *f* = 0.9, E_{SE} = -1.3933 (middle), *f* = 0.82, E_{SE} = -1.31(right))

To further investigate the bounce back motion with decreasing *f*, we can examine the eigen states of the limited case of 4-body system. Assume linearization near the Sun-Mars L_1 and L_2 points. Then the equation of motion can be simplified by following the steps of eigen-analysis previously discussed in section 3.2 (see equation 3.8).

$$\frac{d}{dt}\begin{pmatrix}\tilde{x}\\ y\\ v_x\\ v_y\end{pmatrix}=\begin{bmatrix}0 & 0 & 1 & 0\\ 0 & 0 & 0 & 1\\ a & 0 & 0 & 2\\ 0 & -b & -2 & 0\end{bmatrix}\begin{pmatrix}\tilde{x}\\ y\\ v_x\\ v_y\end{pmatrix} \tag{4.15}$$

where $x = x_L + \tilde{x}$, and $\tilde{x} \ll r_h$. Then the energy integral for the Sun-Mars System:

$$\begin{aligned} E_{S-M} &= \frac{1}{2}\left({v_y}^2 + {v_y}^2\right) + \bar{U}(x,y) \\ &= \tfrac{1}{2}\left({v_y}^2 + {v_y}^2\right) - \tfrac{1}{2}(x^2+y^2) - \frac{f}{R} - \frac{\mu_M}{R_M} \end{aligned} \tag{4.16}$$

Eigenvectors and eigenvalues can be calculated with parameter $\bar{\mu}$.

$$a = -\frac{\partial^2 \bar{U}}{\partial x^2}\Big|_{x=x_L,\, y=0} = 1 + \frac{2f}{|x_L|^3} + \frac{2\mu_M}{|x_L-1|^3} = 1 + 2\bar{\mu} \tag{4.17a}$$

$$b = -\frac{\partial^2 \bar{U}}{\partial y^2}\Big|_{x=x_L,\, y=0} = \frac{f}{|x_L|^3} + \frac{\mu_M}{|x_L-1|^3} - 1 = \bar{\mu} - 1 \tag{4.17b}$$

$$\bar{\mu} = \frac{f}{|x_L|^3} + \frac{\mu_M}{|x_L-1|^3} \tag{4.17c}$$

Eigenvalues and corresponding eigenvectors are:

$$\lambda_{1,2} = \pm\left[\frac{\bar{\mu}-2+\sqrt{9\bar{\mu}^2-8\bar{\mu}}}{2}\right]^{1/2} = \pm\lambda \tag{4.18a}$$

$$\lambda_{3,4} = \pm i\left[\frac{2-\bar{\mu}+\sqrt{9\bar{\mu}^2-8\bar{\mu}}}{2}\right]^{1/2} = \pm i\upsilon \tag{4.18b}$$

$$\begin{bmatrix} u_1 & u_2 & w_1 & w_2 \end{bmatrix} = \begin{bmatrix} 1 & 1 & 1 & 1 \\ -\sigma & \sigma & -i\tau & i\tau \\ \lambda & -\lambda & i\upsilon & -i\upsilon \\ -\lambda\sigma & -\lambda\sigma & \upsilon\tau & \upsilon\tau \end{bmatrix} \tag{4.18c}$$

$$\sigma = \frac{2\lambda}{\lambda^2+b} > 0\,, \quad \tau = -\left(\frac{\upsilon^2+a}{2\upsilon}\right) < 0 \tag{4.18d}$$

Based on the obtained eigenvectors, we can describe the equation of motion for the limited 4-body problem into the first-order form. It is useful to track the contour of the Lyapunov orbit around the Lagrange points. By using the 1-D search technique, the global structure of the invariant manifolds can be mapped simply. Let us explore the significant changes in the configuration of the invariant manifolds when the factor *f* is decreased. As an example, we tracked the centerline of the invariant manifolds near the Sun-Mars L_2 point while the factor *f* is decreased. The initial conditions for each case of unstable and stable manifolds can be obtained from the calculated eigenvalues in the equation 4.18. For case 1, we assumed that the spacecraft left in the exterior realm direction through unstable manifolds starting at the Sun-Mars L_2 point. The initial condition for the case 1 is $(\tilde{x} \quad y \quad v_x \quad v_y)_{t=0} = \alpha[1 \quad -\sigma \quad \lambda \quad -\lambda\sigma]$ so that the S/C can follow the centerline of the unstable manifolds. As seen in Figure 25, the S/C trajectories with different value of *f* are shown in Sun-Mars rotating frame. When the factor *f* is 1, meaning no solar sail effect, the S/C travels like a shape of a scallop shell around the forbidden zone and coms back to the starting point. By deploying the solar sail so that it reduced the value of the factor *f*, the size of the scallop shell gets bigger. Also a number of the bounce back motion by hitting the forbidden zone barrier is reduced during the one cycle of motion. This behavior can be explained by the

relationship between the energy integral and the factor *f*. When *f* is decreased, the criteria of the energy level for E_2 and E_3 are increased. So when the energy level of the entire system still remains the same with no additional thrust, the thickness of the forbidden zone is increased. That increases the size of scallop shell trajectory since the S/C hits the forbidden zone barrier and bounces off slowly during the one cycle of the motion. In Figure 25, the outer radius of the S/C trajectories are increased from 1 to 1.5 by reducing the factor *f*. For case 2, the S/C follows the centerline of the unstable manifolds to the interior realm direction at Sun-Mars L_2 point. The initial condition for case 2 is $(\tilde{x} \quad y \quad v_x \quad v_y)_{t=0} = \alpha[-1 \quad \sigma \quad -\lambda \quad \lambda\sigma]$. In Figure 26, when the factor *f* is 1, the S/C flies near Mars many times to reach the Sun-Mars L_1 point. As *f* is decreased slowly, the S/C trajectory is trapped in a halo orbit between Mars and the Sun-Mars L_2 point. So the S/C cannot connect with the Sun-Mars L_1 point. For case 3, we assumed that the S/C left in the exterior realm direction through stable manifolds starting at Sun-Mars L_2 point. The initial condition for the case 3 is $(\tilde{x} \quad y \quad v_x \quad v_y)_{t=0} = \alpha[1 \quad \sigma \quad \lambda \quad \lambda\sigma]$ while time direction is -1. The S/C trajectories are quite similar to the case 1 as you can see in Figure 27. However, the S/C starts to fly in the opposite direction of case 1. For the last case, the S/C travels through stable manifolds to the interior realm direction starting at the Sun-Mars L_2 point. The initial condition for case 4 is $(\tilde{x} \quad y \quad v_x \quad v_y)_{t=0} = \alpha[-1 \quad -\sigma \quad -\lambda \quad -\lambda\sigma]$ while time direction is -1. The S/C trajectories also show the same behaviors of case 2, but in the opposite direction. In Figure 28, the S/C captured in a halo orbit between Mars and the Sun-Mars L_2 point when the factor *f* is below 0.99.

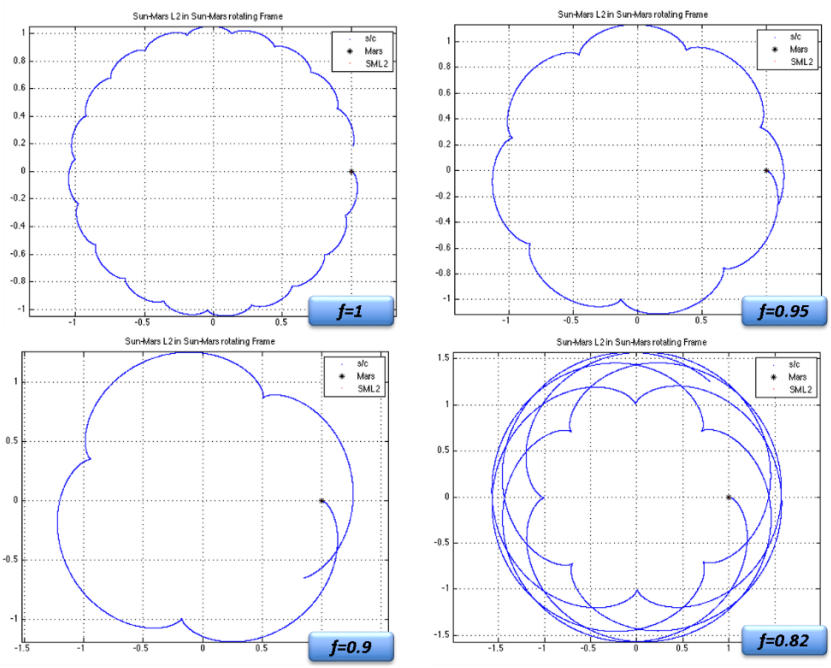

Figure 25. S/C trajectory from the Sun-Mars L_2 point into unstable manifolds to the exterior realm

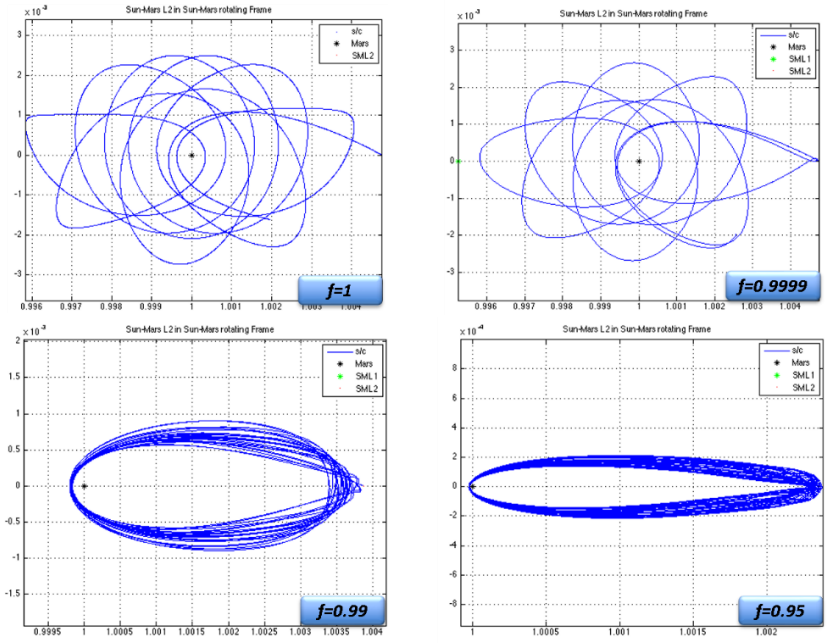

Figure 26. S/C trajectory from the Sun-Mars L_2 point into unstable manifolds to the interior realm

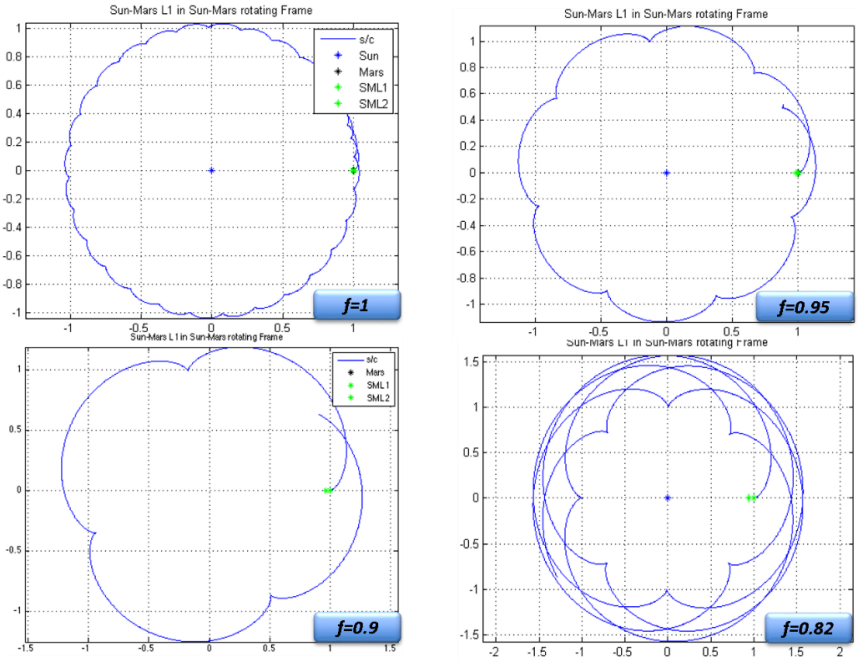

Figure 27. S/C trajectory from the Sun-Mars L_2 point into stable manifolds to the exterior realm

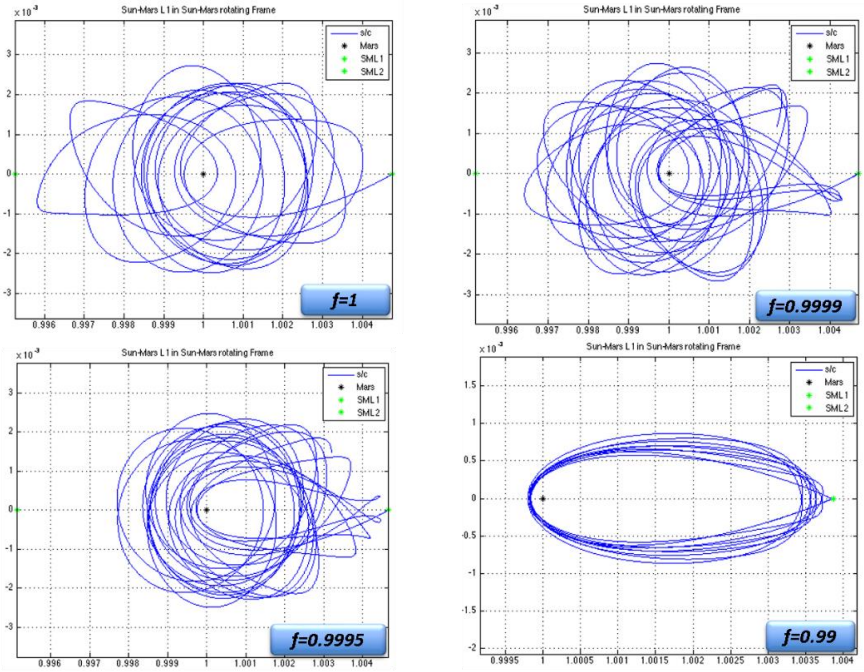

Figure 28. S/C trajectory from the Sun-Mars L_2 point into stable manifolds to the interior realm

4.3 Transfer Trajectory from Earth to Mars with Solar Sail

To avoid any bounce back motion of the S/C trajectory, it is necessary to calculate the required energy to maintain the neck region open for the reduced value of the factor *f*. By tracking the centerline of the invariant manifolds with different *f*, we can have a glimpse of the changes in the global structure of the manifolds. Therefore we can design the advanced transfer trajectory from Earth to Mars by benefiting from these features: 1) when the solar sail is deployed, it cancels the Sun's gravitational force by reducing the value of factor *f*; 2) when the factor *f* is reduced, the Sun-Mars Lagrange points are shifted towards the Sun's direction; 3) the criteria of energy to maintain the neck region open are increased with decreasing *f;* 4) the structure of the invariant manifolds which are changed by decreasing *f* can be simply mapped using the 1-D search technique.

To design a transfer trajectory from the Sun-Earth L_2 point to Mars, let us explore the centerline of unstable manifolds with different *f*. Assume that the S/C departs from the Sun-Earth L_2 point through the unstable manifolds to the exterior realm. In Figure 29, when $f = 1$, the S/C trajectory has a scallop shape around the forbidden zone of the Sun-Earth system in Sun-Earth rotating frame. Even if we propagate the trajectory for a long time, the S/C will not reach the Mars orbit. By using the reduced $f = 0.8$ at the time of departure, the S/C trajectory starts to intersect the Mars orbit. If the factor *f* is decreased to below 0.6, the S/C will pass Mars orbit and circle further away from the Sun. In Figure 30, the S/C trajectories with different *f* are shown in the Sun-Mars rotating frame. In the initial state at $f = 1$, the S/C moves around the orbit of Sun-Earth

L_2 points. But when f = 0.9, it starts to show the bounce back motions by hitting the forbidden zone of Sun-Mars system. Especially there are rewind points of the S/C trajectory when f = 0.85. The S/C flies to the Sun-Mars L_2 point and comes back near the Sun-Earth L_2 point again when f = 0.8. This retro trajectory can be useful to transfer to Mars.

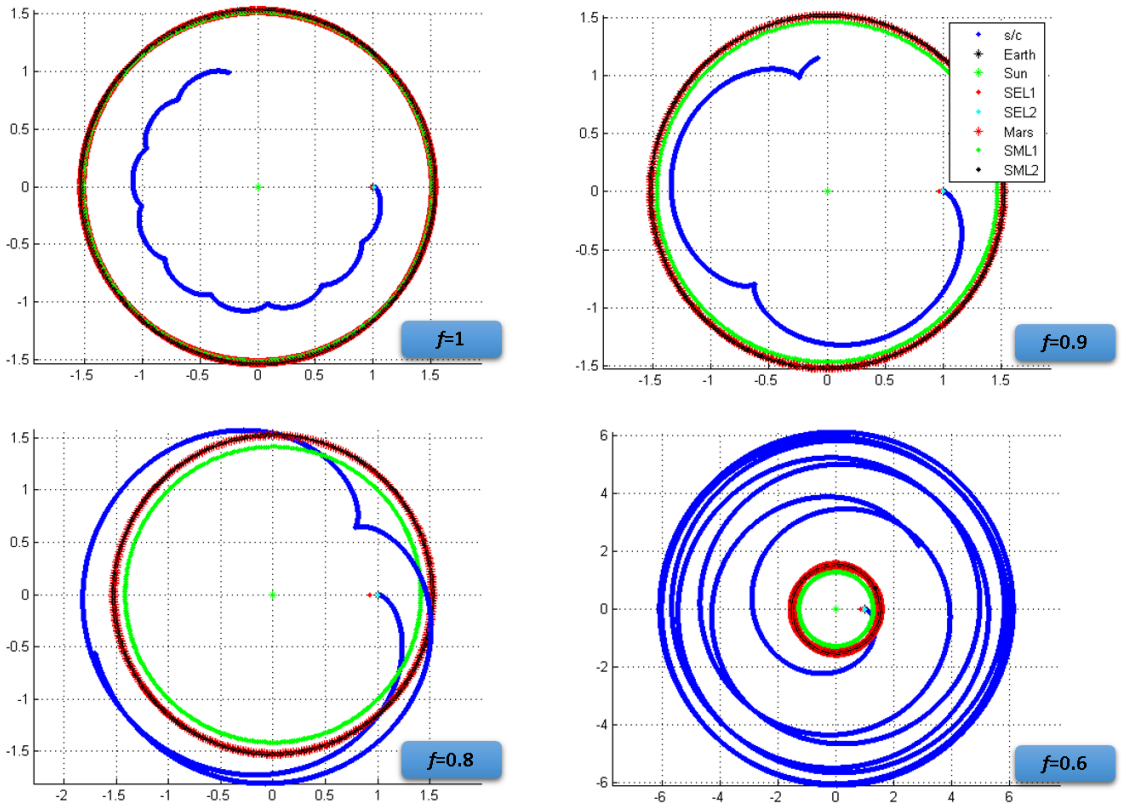

Figure 29. S/C trajectory from the Sun-Earth L_2 point to the Sun-Mars L_1 point in the Sun-Earth rotating frame

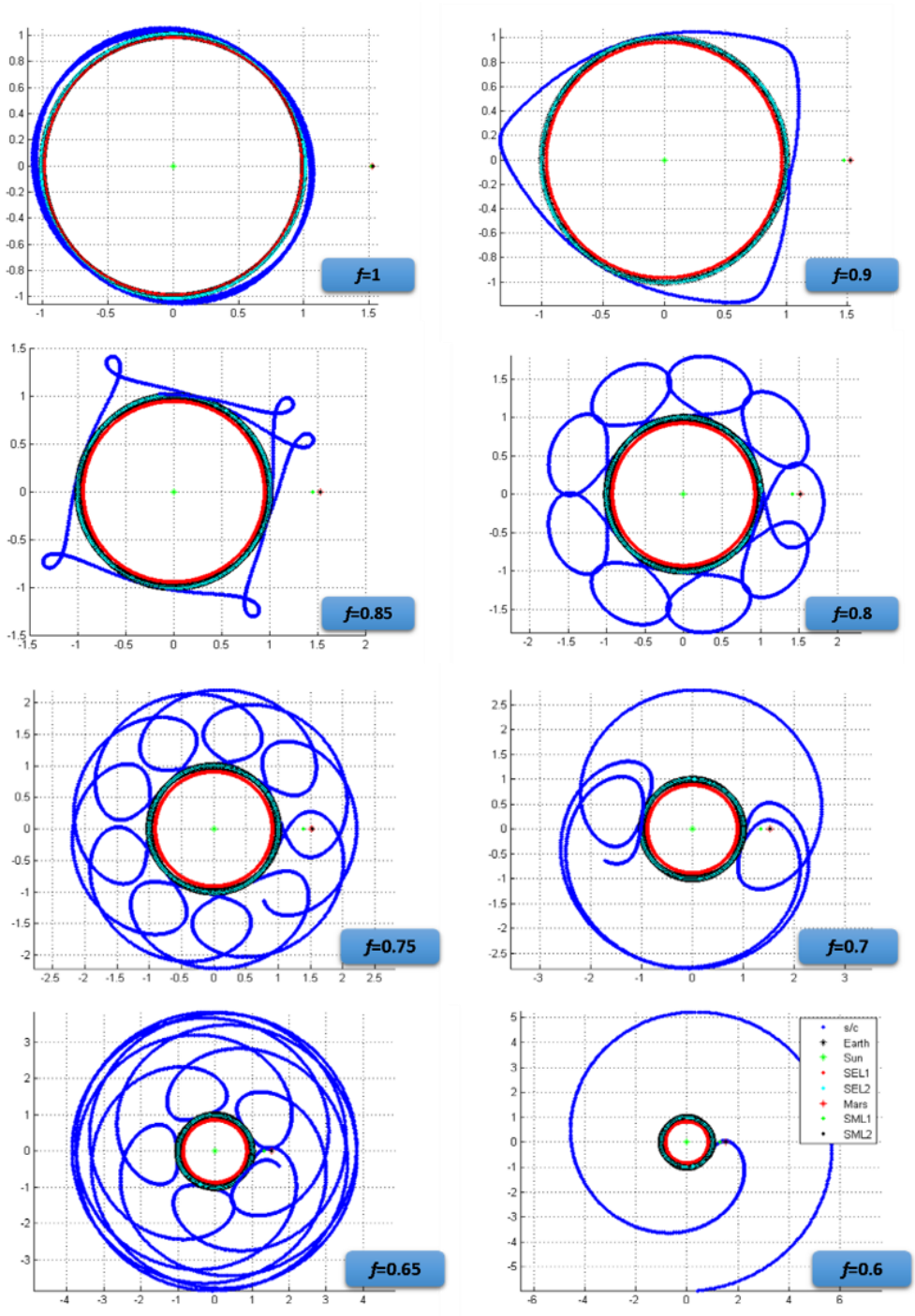

Figure 30. S/C trajectory from the Sun-Earth L_2 point to the Sun-Mars L_1 point in the Sun-Mars rotating frame

By taking advantage of the work described above, an example trajectory from the Sun-Earth L_2 point to Mars can be designed. In this case, we assume that the S/C departs from Earth to the Sun-Earth L_2 point via the Earth-Moon system as in the NEA rendezvous mission described in section 3.3. The initial conditions of the S/C remain the same: the mass of S/C is 1 MT and the specific impulse, I_{sp} is 3000s. As you can see in Figure 31, the S/C escapes from the Sun-Earth L_2 point through the unstable manifolds to the exterior realm and starts to deploy the solar sails. For 1.05 years (=384.3 days), the S/C coasts along the manifolds and then *f* is reduced to 0.9. By reducing *f*, the Sun-Mars Lagrange points are moved toward the Sun and the structure of the manifolds is also changed. After travelling 74.45 days, the factor *f* is reduced to 0.80085. Then the S/C flies over the Sun-Mars L_2 point and turns back toward Mars. The S/C approaches to Mars less than 0.0001396 AU (=2,090 km), below than the Martian geostationary orbit altitude of 13,634 km.

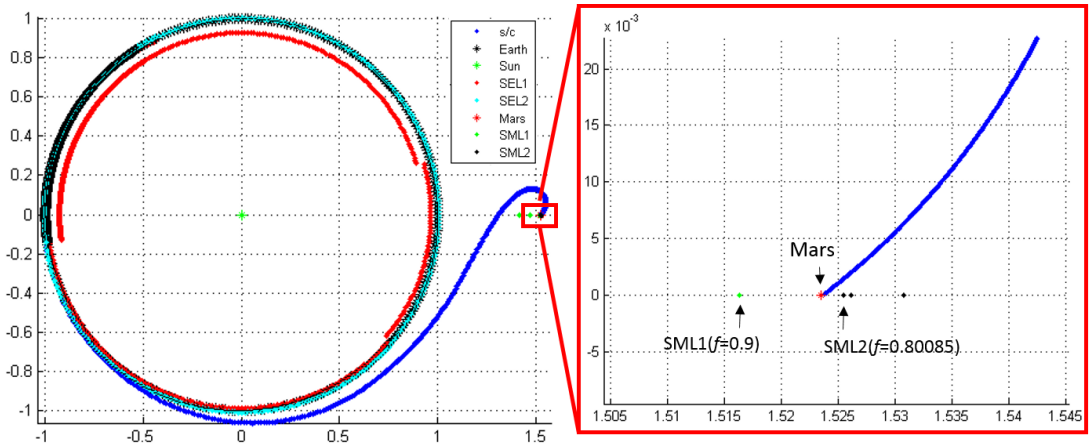

Figure 31. Transfer trajectory from Sun-Earth L_2 point to Mars in Sun-Mars rotating frame

The time of flight for the retro trajectory is 829.6 days. Therefore the total flight time of the transfer trajectory from Earth to Mars is approximately 2.93 years and the energy consumption is only 2.698 km/s. This interesting retro trajectory is achieved without fuel expenditure by using the interplanetary super highway method with solar sail. The summary of the cost is shown in Table 4.

Table 4. Summary of cost for transfer trajectory from Earth to Mars

		TOF [days]	**ΔV [km/s]**
Earth to Sun-Earth L_2 point		239.1	2.698
Sun-Earth L_2 point to Mars	$f = 1$	384.3	0
	$f = 0.9$	74.45	0
	$f = 0.80085$	370.8	0
		829.6	0
Total		1068.7 (=2.93 yrs)	2.698

5. SUMMARY AND FUTURE WORK

The overall purpose of this paper is to develop advanced mission design with interplanetary transfer trajectory methods which can provide the minimum fuel cost for complex and long duration space missions. To develop this new low-energy trajectory method, called IPSH method, the dynamical properties of the PCR3BP were considered. Also it was essential to explore the characteristics of the invariant manifolds winding around the Lagrange points in the three-body system. With understanding of dynamical symmetries and energy state dynamics, computationally simplified methods for IPSH trajectory designs can be achieved. A simple method, called 1-D search technique, can depict the centerline of the invariant manifolds issuing from the periodic orbits around the Lagrange points. It allows us to see at a glance the global structure of the invariant manifolds. For a meaningful design exercise, NEAs rendezvous mission was discussed in four phases. In phase 1, a 1MT spacecraft slowly spiraled away from Earth LEO to Earth-Moon L_1 point by using small thrust. Then the S/C followed the thrust-free trajectory to reach Earth-Moon L_2 point in phase 2. By considering four-body dynamics into two segments of three-body dynamics, the system-to-system transfer trajectory from Earth-Moon L_2 point to Sun-Earth L_2 point were described in phase 3. Lastly, the S/C travelled the grand tour of the NEAs by executing small burns and coasting stable/unstable manifolds and returned back to Sun-Earth L_2 point. The total trip time is 843.6 days with $\Delta V = 8.406\ \mathrm{km/s}$.

For a second application study, the Mars exploration mission with solar sail was considered. The propulsive power obtained from the solar sail can affect the three-body dynamics by changing the geometry of invariant manifolds near the Lagrange points. A limited case for four-body system was formulated with Earth, Mars, and S/C while Sun is at origin. The significant changes in energy state and manifold structure due to the solar sail factor *f* were investigated in depth. Therefore, we found that those changes can be useful to design energy efficient trajectories for various interplanetary space mission. As an example, a thrust-free trajectory from the Sun-Earth L_2 point to Mars was developed.

This research contributed to broaden the understanding of the natural dynamics of the solar system and to design advanced transfer trajectories with significantly reduced ΔV. The developed 1-D search technique can efficiently reveal the geometrical framework for the whole tube-structure of the invariant manifolds based on the centerline. With extended research on the general solution of the multi-body problem and the effect of solar sails, it can be possible to develop an advanced design tool of low-thrust trajectory for various interplanetary space missions.

REFERENCES

[1] W. S. Koon, M. W. Lo, J. E. Marsden and S. D. Ross, *Dynamical Systems, the Three-Body Problem, and Space Mission Design*, Berlin, Springer, 2008

[2] M. W. Lo, "The Interplanetary Superhighway and the Origins Program," Aerospace Conference Proceedings, IEEE, Vol. 7, pp. 7-3543, 2002

[3] W. S. Koon, M. W. Lo, J. E. Marsden and S. D. Ross, "Shoot the Moon," AAS 00-166, AAS/AIAA Astrodynamics Specialist Conference, 2000

[4] S. D. Ross, "Cylindrical Manifolds and Tube Dynamics in the Restricted Three-Body Problem," Ph.D. Dissertation, California Institute of Technology, 2004

[5] V. G. Szebehely, *Adventures in Celestial Mechanics, a First Course in the Theory of Orbits*, Austin, University of Texas Press, 1989

[6] H. Schaub and J. L. Junkins, *Analytical Mechanics of Space Systems*, Reston, VA, AIAA, 2nd ed., 2009.

[7] V. G. Szebehely, *Theory of Orbits*, Academic Press, New York, 1967

[8] G. W. Hill, "Mr. Hill's Researches in the Lunar Theory," Monthly Notices of the Royal Astronautical Society, Vol. 39, pp. 258-261, November 1879

[9] J. Barrow-Green, *Poincare and the Three Body Problem*, Providence RI, American Mathematical Society, History of Mathematics, Vol. 2, 1997

[10] R. W. Farquhar, D. P. Muhonen, C. R. Newman, and H. S. Heuberger, "Trajectories and Orbital Maneuvers for the First Libration-Point Satellite," Journal of Guidance and Control, Vol. 3, pp. 549-554, November-December 1980

[11] R. W. Farquhar, "The Flight of ISEE-3/ICE: Origins, Mission History, and a Legacy," AIAA Paper 98-4464, AIAA/AAS Astrodynamics Specialist Conference and Exhibit, August 1998

[12] K. C. Howell, B. T. Barden, R. S. Wilson, and M. W. Lo, "Trajectory Design Using a Dynamical Systems Approach with Applications to Genesis,", Advances in the Astronautical Sciences, Vol. 97, Part II, pp.1665-1684, 1997

[13] E. A. Belbruno, *Capture Dynamics and Chaotic Motions in Celestial Mechanics*, Princeton, NJ, Princeton University Press, 2004

[14] E. A. Belbruno and J. K. Miller, "Sun-Perturbed Earth-to-Moon Transfers with Ballistic Capture," Journal of Guidance, Control, and Dynamics, Vol. 16, No. 4, pp. 770-775, 1993.

[15] B. T. Barden and K. C. Howell, "Fundamental Motions Near the Collinear Libration Points and Their Transitions," Journal of the Astronautical Sciences, Vol. 46, No.4, pp. 361-378, 1998

[16] C. C. Conley, "Low Energy Transit Orbits in the Restricted Three-Body Problem," SIAM J. Appl. Math., Vol. 16, pp. 732–746, 1968

[17] J. E. Prussing and B. A. Conway, *Orbital Mechanics*, Oxford, Oxford University Press, 1993

[18] M. W. Lo and S. D. Ross, *The Lunar L1 Gateway: Portal to the Stars and Beyond*, Pasadena, CA: Jet Propulsion Laboratory, National Aeronautics and Space Administration, 2001

[19] K. C. Howell, B. T. Barden and M. W. Lo, "Application of Dynamical Systems Theory to Trajectory Design for a Lagrange Point Mission," Journal of Astronautial Sciences, Vol. 45, No. 1, pp. 161-178, 1977

[20] R. R. Rausch, "Earth to Halo Orbit Transfer Trajectories", M.S. Thesis, School of Aeronautics and Astronautics, Purdue University, 2005

[21] J. D. Mireles James, "Celestial Mechanics Notes Set 5: Symmetric Periodic Orbits of the Circular Restricted Three Body Problem and their Stable and Unstable Manifolds," Rutgers University, 2006

[22] R. McGehee, "Some Homoclinic Orbits for the Restricted Three-Body Problem," Ph.D. Dissertation, University of Wisconsin, Madison, 1969

[23] G. Gomez, W. S. Koon, M. W. Lo, J. E. Marsden, J. Masdemont, and S. D. Ross, "Invariant Manifolds, the Spatial Three-Body Problem and Space Mission Design," AAS 01-301, AAS Conference, August 2001

[24] D. B. Kanipe, D. C. Hyland, "Investigation of the Potential for Human Travel into Deep Space Using Current, or Imminently, Available Technology," AIAA 2014-4238, AIAA Space 2014 Conference, August 4-7, 2014

[25] G. P. Alonso, "The Design of System-to-System Transfer Arcs using Invariant Manifolds in the Multi-body Problem", Ph.D. Dissertation, Purdue University, 2006

[26] F. Topputo, M. Vasile and A. E. Finzi, "Combining Two and Three-Body Dynamics for Low Energy Transfer Trajectories of Practical Interest," Proceedings of the 55th International Astronautical Congress, pp. 584-596, 2004

[27] J. Lu, M. Zhang, Q. Lu, “Transfer Trajectory Design for Mars Exploration,” International Journal of Astronomy and Astrophysics, Vol. 3, No. 2A, pp. 5-16, 2013